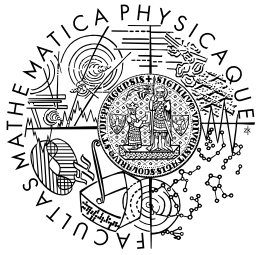

FACULTY
OF MATHEMATICS
AND PHYSICS
Charles University

BACHELOR THESIS

Ondřej Zelenka

Chaotic motion in Johannsen-Psaltis spacetime

Institute of Theoretical Physics

Supervisor of the bachelor thesis:	Loukes Gerakopoulos Georgios, Dr.
Study programme:	Physics
Study branch:	General Physics

Prague 2017

I declare that I carried out this bachelor thesis independently, and only with the cited sources, literature and other professional sources.

I understand that my work relates to the rights and obligations under the Act No. 121/2000 Sb., the Copyright Act, as amended, in particular the fact that the Charles University has the right to conclude a license agreement on the use of this work as a school work pursuant to Section 60 subsection 1 of the Copyright Act.

In ..... date ..... signature of the author

Název práce: Chaotický pohyb v prostoročase Johannsen-Psaltis

Autor: Ondřej Zelenka

Ústav: Ústav teoretické fyziky

Vedoucí bakalářské práce: Loukes Gerakopoulos Georgios, Dr., Ústav teoretické fyziky

Abstrakt: Johannsen-Psaltis je perturbace Kerrova prostoročasu navržená tak, aby neobsahovala patologie jako nahé singularity a uzavřené časupodobné křivky. Tento prostoročas závisí nejen na hmotnosti a momentu hybnosti centrálního objektu, ale také na dalších parametrech, kterými se odlišuje od Kerrova; v této práci uvažujeme jen fyzikální parametr nejnižšího řádu. V této práci shrneme základy teorie regulární a chaotické dynamiky a na numerických příkladech ukážeme, že geodetický pohyb v tomto prostoročase může vykazovat chaotické chování. Studujeme příslušný fázový prostor pomocí Poincarého řezů a rotačních čísel, abychom ukázali chaotické chování jak přímo, tak nepřímo (např. pomocí Birkhoffových řetezů), a použijeme Lyapunovovy exponenty, abychom přímo odhadli citlivost na počáteční podmínky.

Klíčová slova: chaos, geodetický pohyb, černé díry

Title: Chaotic motion in Johannsen-Psaltis spacetime

Author: Ondřej Zelenka

Institute: Institute of Theoretical Physics

Supervisor: Loukes Gerakopoulos Georgios, Dr., Institute of Theoretical Physics

Abstract: The Johannsen-Psaltis spacetime is a perturbation of the Kerr spacetime designed to avoid pathologies like naked singularities and closed timelike curves. This spacetime depends not only on the mass and the spin of the central object, but also on extra parameters, making the spacetime deviate from Kerr; in this work we consider only the lowest order physically meaningful extra parameter. In this thesis we summarize the basics of the theory of regular and chaotic dynamics and we use numerical examples to show that geodesic motion in this spacetime can exhibit chaotic behavior. We study the corresponding phase space by using Poincaré sections and rotation numbers to show chaotic behavior both directly and indirectly (e.g. Birkhoff chains), and we use Lyapunov exponents to directly estimate the sensitivity to initial conditions for chaotic orbits.

Keywords: chaos, geodesic motion, black holes

I would like to thank my supervisor Georgios Loukes Gerakopoulos and consultant Petra Suková for all their help, guidance and patience.

Contents

Introduction

In this thesis we study the geodesic motion in a metric constructed by Johannsen and Psaltis in [1]. This metric describes a family of spacetimes characterized by an infinite number of parameters, i.e. the mass M, the spin a and a series of deviation parameters ϵ_k, where $k \in \mathbb{N}_0$. However, in this thesis we constrain ourselves to the lowest order of the unconstrained parameters, which is ϵ_3.

The Johannsen-Psaltis metric was designed to be a perturbation of the Kerr spacetime, which is of great astrophysical interest. The so-called *no-hair theorem* [2] states that the class of uncharged black-hole exterior solutions which are axisymmetric and don't violate causality (i.e. no closed timelike or null curves) consists of a discrete set of continuous families, each depending on at least one and at most two independent parameters. No other externally observable parameters are required. Typically the Kerr type is assumed [3] and such black holes are parametrized by their mass M and their angular momentum a. However, there is yet to be mathematical proof of this (this is why mathematicians call it the *no-hair conjecture*). It would be of great astrophysical interest to test this conjecture by observing black hole candidates and verifying that the electromagnetic and gravitational wave signals do not deviate from the ones corresponding to Kerr spacetimes.

One of the characteristics of the Kerr spacetime background is that geodesic motion in such a background is integrable [4]. Many of the non-Kerr spacetimes, by which term we denote perturbations of the Kerr spacetime, do not possess the symmetry that the Kerr spacetime does, making geodesic motion lose one of its integrals of motion. This causes geodesic motion in such a spacetime to exhibit chaotic behavior, which we study in this thesis.

The organization of the thesis is as follows: in the first chapter we describe the basics of geodesic motion and deterministic chaos in dynamical systems; we will already discuss some of the properties of the studied spacetime. In the second chapter we use numerical examples to show that the Johannsen-Psaltis metric indeed doesn't possess the final integral of motion.

1. Theoretical foundations

1.1 Notation and conventions

As this thesis lies in the field of general relativity, we use the standard abstract index notation. We denote the covariant metric tensor $g_{\mu\nu}$ and its contravariant version $g^{\mu\nu}$. The corresponding matrices are mutually inverse, which is expressed by the identity

$$\sum_{\nu} g_{\mu\nu} g^{\nu\sigma} = \delta_{\mu}{}^{\sigma}, \tag{1.1}$$

where $\delta_{\mu}{}^{\sigma}$ denotes the Kronecker delta symbol, which is equal to 1 for $\mu = \sigma$ and equal to zero in the other cases. We also use the standard summation convention, so in expressions we omit the symbol for the sum over any index which goes over all its possible values and appears once as a covariant and once as a contravariant index in a product. Therefore, the previous equation can be written simply as

$$g_{\mu\nu} g^{\nu\sigma} = \delta_{\mu}{}^{\sigma}. \tag{1.2}$$

The metric fully describes the local geometry of the corresponding spacetime, its signature is (-,+,+,+) by convention. We use geometric units, i.e. $c = G = 1$ (c is the speed of light, G is the gravitational constant).

For now, we mark the coordinates of the spacetime x^{μ}, where we limit ourselves to four-dimensional spacetimes, therefore the index μ can have the values 0, 1, 2 and 3. While the primary use of the index 0 is to denote the time variable, the general theory of relativity is fully covariant and so no coordinate must necessarily play the role of time. Later on, when we work with a specific spacetime, we will use a different notation. Greek indices will be used to denote tensor components. A Latin letter as a superscript will typically be a power; the exception is an object which is already defined with an index (e.g. W^u and W^s in Sec. 1.10).

If we take any differentiable function from the spacetime manifold to the real numbers, we denote the partial derivative

$$A_{,\mu} := \frac{\partial A}{\partial x^{\mu}}. \tag{1.3}$$

We now denote

$$\Gamma_{\alpha\mu\nu} := \frac{1}{2} \left(g_{\alpha\mu,\nu} + g_{\nu\alpha,\mu} - g_{\mu\nu,\alpha} \right) \tag{1.4}$$

the Christoffel symbols of the first kind and

$$\Gamma^{\beta}{}_{\mu\nu} := g^{\alpha\beta} \Gamma_{\alpha\mu\nu} \tag{1.5}$$

the Christoffel symbols of the second kind.

1.2 The Johannsen-Psaltis spacetime

In this thesis we work with the metric constructed for rapidly spinning black holes introduced by Johannsen and Psaltis in [1]. In Boyer-Lindquist-like coordinates it's given by the line element

$$\mathrm{d}s^2 = g_{tt}\mathrm{d}t^2 + g_{rr}\mathrm{d}r^2 + g_{\theta\theta}\mathrm{d}\theta^2 + g_{\phi\phi}\mathrm{d}\phi^2 + 2g_{t\phi}\mathrm{d}t\mathrm{d}\phi. \tag{1.6}$$

In order to write the metric components $g_{\mu\nu}$ in a fairly simple fashion we use several metric functions as used in [1]

$$\Sigma = r^2 + a^2 \cos^2\theta, \tag{1.7a}$$

$$h = \sum_{k=0}^{\infty} \left(\epsilon_{2k} + \epsilon_{2k+1} \frac{Mr}{\Sigma}\right) \left(\frac{M^2}{\Sigma}\right)^k, \tag{1.7b}$$

$$\Delta = r^2 + a^2 - 2Mr, \tag{1.7c}$$

$$\omega^2 = r^2 + a^2, \tag{1.7d}$$

$$\Lambda = \omega^4 - a^2 \Delta \sin^2\theta, \tag{1.7e}$$

which simplify the task of writing the metric components. In order to also simplify the task of calculating second partial derivatives of the metric components we define even more metric functions

$$B := \Delta + a^2 h \sin^2\theta, \tag{1.8a}$$

$$C := \frac{\Lambda \sin^2\theta}{\Sigma}, \tag{1.8b}$$

$$F := 1 + \frac{2Mr}{\Sigma}, \tag{1.8c}$$

$$D := h a^2 F \sin^4\theta, \tag{1.8d}$$

which will then along with their first and second derivatives appear in the first and second partial derivatives of the metric components. While we omit the arguments of the functions for simplicity (e.g. we write Σ instead of $\Sigma(r,\theta)$), it is important to keep in mind that they are still generally functions of r and θ.

Now that we have defined these metric functions, we can write the metric components

$$g_{tt} = -(1+h)\left(1 - \frac{2Mr}{\Sigma}\right), \tag{1.9a}$$

$$g_{t\phi} = -\frac{2aMr\sin^2\theta}{\Sigma}(1+h), \tag{1.9b}$$

$$g_{\phi\phi} = C + D, \tag{1.9c}$$

$$g_{rr} = \frac{\Sigma(1+h)}{B}, \tag{1.9d}$$

$$g_{\theta\theta} = \Sigma. \tag{1.9e}$$

The function $h(r,\theta)$ is what causes the deviation from the Kerr metric, as setting $\epsilon_k = 0 \quad \forall k \in \mathbb{N}_0$ gives the Kerr metric. The parameters $(\epsilon_k)_{k=0}^{\infty}$ are, however, constrained. As explained in detail in [1], in stationary asymptotically flat spacetimes the deviation from the flat solution must fall off as r^{-2} or faster, while non-zero values of ϵ_k parameters generate $\mathcal{O}\left(r^{-k}\right)$ terms, we therefore set $\epsilon_0 = \epsilon_1 = 0$. The parameter ϵ_2 is constrained by observational constraints on weak-field deviations from general relativity [1] as $|\epsilon_2| \leq 4.6 \cdot 10^{-4}$. We set this one to be zero as well and limit ourselves to the lowest order remaining parameter, which is ϵ_3, and set all the higher order parameters $\epsilon_k = 0 \quad \forall k \geq 4$. The function h then takes the form

$$h = \epsilon_3 \frac{M^3 r}{\Sigma^2}. \tag{1.10}$$

1.3 Lagrangian mechanics

We will keep using Greek indices and the summation convention for consistency.

For a typical mechanical system evolving along the time parameter τ, we can define generalized coordinates q^μ, which characterize the location of the system. These coordinates can have the meaning of angles, distances, spatial coordinates and so on. In order to fully characterize the state of the system, we need to add the generalized velocities $\dot{q}^\mu := \mathrm{d}q^\mu/\mathrm{d}\tau$. For classical conservative mechanical systems we use the kinetic energy T and the potential energy V and we take a function on the space of generalized coordinates, generalized velocities and time

$$\mathcal{L}\left(q^\mu, \dot{q}^\mu, \tau\right) = T\left(q^\mu, \dot{q}^\mu, \tau\right) - V\left(q^\mu, \tau\right). \tag{1.11}$$

The motion of the system is then described using the *principle of least action*, which states that for fixed τ_1, τ_2, $q^\mu\left(\tau_1\right)$ and $q^\mu\left(\tau_2\right)$ the trajectory of the system is a stationary point of the *action* functional

$$S = \int_{\tau_1}^{\tau_2} \mathcal{L}\left(q^\mu, \dot{q}^\mu, \tau\right) \mathrm{d}\tau, \tag{1.12}$$

the equations of motion take on the form of the Euler-Lagrange equations (in this case also called the Lagrange equations of the second kind)

$$\frac{\mathrm{d}}{\mathrm{d}\tau}\left(\frac{\partial \mathcal{L}}{\partial \dot{q}^\mu}\right) - \frac{\partial \mathcal{L}}{\partial q^\mu} = 0. \tag{1.13}$$

This description can be used for relativistic systems as well. If we take a trajectory $x^\mu = x^\mu\left(\tau\right)$, where τ parametrizes the corresponding curve on the spacetime manifold, we will first need an invariant measure of time. A typical choice is the proper time

$$\left(\mathrm{d}\tau\right)^2 := -g_{\mu\nu}\mathrm{d}x^\mu \mathrm{d}x^\nu \tag{1.14}$$

(which will also prove to be an efficient choice). The proper time is the time that an observer moving along the trajectory would measure on his own watch. If we take a trajectory of a particle on the spacetime manifold and parametrize it by the proper time, we will denote the derivative of a differentiable quantity by the proper time

$$\dot{A} = \frac{\mathrm{d}A}{\mathrm{d}\tau}. \tag{1.15}$$

The definition of the proper time (1.14) causes the following identity to hold

$$g_{\mu\nu}\dot{x}^\mu \dot{x}^\nu = -1. \tag{1.16}$$

Now we can write the Lagrangian of a free particle of rest mass m [5]

$$\mathcal{L}\left(x^\mu, \dot{x}^\mu\right) = \frac{m}{2} g_{\mu\nu}\dot{x}^\mu \dot{x}^\nu. \tag{1.17}$$

The corresponding equations of motion (1.13) indeed give the standard form of the geodesic equation

$$\ddot{x}^\mu + \Gamma^\mu{}_{\kappa\lambda}\dot{x}^\kappa \dot{x}^\lambda = 0. \tag{1.18}$$

1.4 Hamiltonian mechanics

Once a system has been formulated as a Lagrangian system, it is easy to move to another formalism, more fitting for the needs of this thesis. This is the Hamiltonian formalism. We first define the canonical momenta

$$p_\mu := \frac{\partial \mathcal{L}}{\partial \dot{q}^\mu}, \tag{1.19}$$

express the generalized velocities as $\dot{q}^\mu \left(q^\mu, p_\mu, \tau\right)$ functions of the coordinates, momenta and time. If the condition

$$\det\left(\frac{\partial p_\mu}{\partial \dot{q}^\nu}\right) \neq 0 \tag{1.20}$$

holds, then we write the Hamiltonian function as a Legendre transform of $\mathcal{L}$ with respect to the generalized velocities

$$\mathcal{H}\left(q^\mu, p_\mu, \tau\right) = p_\nu \dot{q}^\nu \left(q^\mu, p_\mu, \tau\right) - \mathcal{L}\left(q^\mu, \dot{q}^\mu \left(q^\mu, p_\mu, \tau\right), \tau\right). \tag{1.21}$$

The equations of motion then gain the *canonical form*

$$\dot{q}^\mu = \frac{\partial \mathcal{H}}{\partial p_\mu}, \tag{1.22a}$$

$$\dot{p}_\mu = -\frac{\partial \mathcal{H}}{\partial q^\mu}. \tag{1.22b}$$

The $2N$-dimensional set of all possible states of the system (q^μ, p_μ) is then called the *phase space* $\mathcal{X}$. If the Hamiltonian is explicitly independent of time ($\partial\mathcal{H}/\partial\tau = 0$), the system is then called *autonomous*.

If we perform this for the geodesic motion Lagrangian (1.17), we get the canonical momenta

$$p_\mu = \frac{\partial \mathcal{L}}{\partial \dot{x}^\mu} = m g_{\mu\nu} \dot{x}^\nu \tag{1.23}$$

and the Hamiltonian is

$$\mathcal{H} = \frac{1}{2m} g^{\mu\nu} p_\mu p_\nu. \tag{1.24}$$

It is easy to verify that Hamilton's equations of motion (1.22) with the Hamiltonian (1.24) again give the geodesic equation (1.18). As we only study geodesic motion, the rest mass of the test particle doesn't play any role in the equations of motion, therefore we can set the rest mass to be equal to 1 for simplicity and we get

$$\mathcal{H}\left((x^\mu, p_\mu, \tau\right) = \frac{1}{2} g^{\mu\nu}\left(x^\mu\right) p_\mu p_\nu. \tag{1.25}$$

It is important to note that while motion of an uncharged spinless test particle in a gravitational field in classical mechanics is described by a Hamiltonian system with 3 degrees of freedom for spatial coordinates, in general theory of relativity the equations of motion have to be invariant under coordinate transformation on the spacetime manifold. This is why the corresponding Hamiltonian system has 4 degrees of freedom - 3 for spatial coordinates and 1 for the coordinate time parameter and the proper time of the particle is taken as the evolution parameter, again, to secure the invariance of the equations. This means that the system is formally autonomous even in non-stationary spacetimes.

1.5 Integrals of motion

In a Hamiltonian system, for a pair of differentiable functions defined on the phase space $A(q^\mu, p_\mu, \tau)$ and $B(q^\mu, p_\mu, \tau)$, we define the Poisson bracket

$$\{A, B\} := \frac{\partial A}{\partial q^\mu}\frac{\partial B}{\partial p_\mu} - \frac{\partial A}{\partial p_\mu}\frac{\partial B}{\partial q^\mu}. \tag{1.26}$$

We can then see that the derivative of such a quantity along the trajectory of the system can be written as

$$\dot{A} = \frac{\partial A}{\partial \tau} + \{A, \mathcal{H}\}. \tag{1.27}$$

It is interesting to note that this allows us to write the equations of motion as

$$\dot{q}^\mu = \{q^\mu, \mathcal{H}\}, \tag{1.28a}$$
$$\dot{p}_\mu = \{p_\mu, \mathcal{H}\}. \tag{1.28b}$$

It also causes any quantity A that doesn't explicitly depend on time and satisfies $\{A, \mathcal{H}\} = 0$ to remain constant during the time evolution of the system. We call such a quantity an *integral of motion*.

We note that the Poisson bracket is antisymmetric ($\{A, B\} = -\{B, A\}$), resulting in the identity $\{A, A\} = 0$. This means that $\{\mathcal{H}, \mathcal{H}\} = 0$, thus in autonomous systems from (1.27) follows that the Hamiltonian is an integral of motion. If we also assume the spacetime metric does not depend on one of the coordinate parameters x^μ, then the corresponding canonical momentum p_μ is an integral of motion. It can be more easily seen from Hamilton's equations (1.22) and the Hamiltonian (1.25). This is in correspondence with Noether's theorem, which says that symmetries of a system cause integrals of motion to exist, and can be associated with the existence of a Killing vector field $\partial/\partial x^\mu$ in differential geometry.

In our spacetime the metric components are independent of the coordinates t and ϕ, making p_t and p_ϕ integrals of motion. We denote

$$E := -p_t, \tag{1.29a}$$
$$L_z := \ \ p_\phi. \tag{1.29b}$$

This symmetry allows us to reduce the system from 4 to 2 degrees of freedom. The dynamics of these two degrees of freedom (t, ϕ) are fairly trivial, we will therefore study the dynamics of the other two degrees of freedom (r, θ). It is easy to see that the reduced Hamiltonian

$$\mathcal{H} = \frac{1}{2}\left(\frac{g_{\phi\phi}E^2 + 2g_{t\phi}EL_z + g_{tt}L_z^2}{g_{tt}g_{\phi\phi} - g_{t\phi}^2} + \frac{p_r^2}{g_{rr}} + \frac{p_\theta^2}{g_{\theta\theta}}\right). \tag{1.30}$$

gives the same equations of motion for the two non-trivial degrees of freedom as the full Hamiltonian (1.25). By this procedure, the integrals (1.29) have been reduced to constant functions in the reduced phase space, making them trivial. However, $\mathcal{H}$ remains a non-trivial function in the reduced phase space. It is to be noted that generally, if an integral is found, simply entering it into the Hamiltonian gives a Hamiltonian which does not generate equivalent dynamics. The case that the canonical momenta themselves are integrals is an exception.

1.6 Canonical transformations

Definition 1 (Canonical transformations)**.** *Let the phase space $\mathcal{X}$ of a Hamiltonian system with the Hamiltonian $\mathcal{H}$ be parametrized by the time τ, coordinates q^μ and the canonical momenta p_μ. We call a canonical transformation any reparametrization of $\mathcal{X}$ using new variables $\bar{q}^\mu$, $\bar{p}_\mu$, in which the equations of motion retain the canonical form*

$$\dot{\bar{q}}^\mu = \frac{\partial \bar{\mathcal{H}}}{\partial \bar{p}_\mu}, \tag{1.31a}$$

$$\dot{\bar{p}}_\mu = -\frac{\partial \bar{\mathcal{H}}}{\partial \bar{q}^\mu}. \tag{1.31b}$$

The point of Hamilton-Jacobi theory is to find a canonical transformation to a set of variables in which the Hamiltonian is $\bar{\mathcal{H}} = 0$, making the motion trivial, determined by $2N$ integration constants identical to $\bar{q}^\mu$, $\bar{p}_\mu$. It is shown in [6] that for the action S in Eq. (1.12)

$$\mathcal{H}\left(q^\mu, p_\mu, \tau\right) + \frac{\partial S}{\partial \tau} = 0 \tag{1.32}$$

holds. Replacing the canonical momenta, we get the *Hamilton-Jacobi equation*

$$\mathcal{H}\left(q^\mu, \frac{\partial S}{\partial q^\mu}, \tau\right) + \frac{\partial S}{\partial \tau} = 0. \tag{1.33}$$

Like Hamilton's canonical equations, the Hamilton-Jacobi equation is the basis of a general method of integrating the equations of motion.

1.7 Integrability, action-angle variables

The Hamilton-Jacobi equation is usually hard to solve, often more complex than solving the respective equations of motion. In some cases, however, it is separable. This means that the function S can be separated completely as a sum of one-variable functions as

$$S\left(q^\mu, \tau\right) = \sum_\nu S_\nu\left(q^\nu\right) - K\tau. \tag{1.34}$$

In this case, *action-angle variables* I_μ, θ^μ can be defined as shown in [7], in which the Hamiltonian is a function of only the momenta

$$\mathcal{H} = \mathcal{H}\left(I_\mu\right), \tag{1.35}$$

making them constants of the motion. θ^μ then evolve as linear functions of time and the motion is restricted to an N-torus.

We call a set of N integrals $\{I_\mu\}$ independent if their gradients span an N-dimensional vector space at each point in phase space. The main result of this is the following theorem [8]:

Theorem 1 (Liouville-Arnol'd theorem)**.** *If there are N independent integrals in involution ($\{I_\mu, I_\nu\} = 0 \quad \forall \mu, \nu$), then the motion lies on a nested family of*

N-dimensional tori, and there exist angle coordinates θ^μ such that the evolution of the system can be written in the form

$$\theta^\mu(\tau) = \theta^\mu(0) + \tau\omega^\mu(I_\nu), \tag{1.36a}$$
$$I_\mu(\tau) = I_\mu(0). \tag{1.36b}$$

We call such a system integrable.

In an integrable system, if we know the fundamental frequencies ω^μ, we can calculate their ratios ω^μ/ω^ν. In the case that all these ratios are rational numbers, the motion is periodic, as the system returns to its initial state in a finite time; such a state is called a *resonance*. In the case of at least one of them irrational, we call the orbit quasi-periodic, as it never returns to its initial state, but it does return arbitrarily close. In the case of two degrees of freedom, there is only one ratio; in the case of its irrationality the orbit densely covers the torus.

This is the case of geodesic motion in the Kerr metric. The Kerr spacetime possesses an additional more complex symmetry expressed through a Killing tensor field, allowing an additional integral of motion, the so-called Carter constant $\mathcal{K}$, to exist [4]. This makes the geodesic motion integrable, the required four integrals of motion are $\mathcal{H}, E, L_z, \mathcal{K}$. It is important to note that the phase space in that case is not strictly bounded, as trajectories plunging into the central black hole always exist (we consider plunging into the central black hole an escape), and for values of energy $E \geq 0$ escapes to $r \to \infty$ exist. However, there remain many non-escaping bounded trajectories and in these non-escaping regions the Liouville-Arnol'd theorem still holds.

1.8 Symplectic mappings

Definition 2 (Symplectic mapping)**.** *We denote the $N \times N$ identity matrix I_N, the Poisson tensor in respect to q^μ, p_μ variables*

$$J_{2N} = \begin{pmatrix} 0 & -I_N \\ I_N & 0 \end{pmatrix} \tag{1.37}$$

and the Jacobi matrix M of the map Ω (also called the monodromy matrix). We call the map Ω in a simply connected phase space $\mathcal{S}$ symplectic, if it fulfills the symplectic condition

$$M^T J_{2N} M = J_{2N}. \tag{1.38}$$

In the case that the phase space $\mathcal{S}$ is a cylinder parametrized by (x, y), where x is the angle coordinate, we call the map $\Omega : (x, y) \mapsto (x', y')$ a twist map, if there is a K such that

$$\left.\frac{\partial x'}{\partial y}\right|_x \geq K > 0. \tag{1.39}$$

Even though the point of this thesis is to study a system with continuous time evolution, it is of great interest to study a discrete mapping as well. In the $2N$-dimensional phase space $\mathcal{X}$ of an autonomous Hamiltonian system the motion lies on the $2N-1$-dimensional surface $\mathcal{E}$ of constant $\mathcal{H}$. If we define a $2N-1$-dimensional surface $\mathcal{Q}$ which is everywhere transversal to the flow, we

can define a mapping Ω on $\mathcal{S} = \mathcal{E} \bigcap \mathcal{Q}$. The transversality of $\mathcal{Q}$ causes $\mathcal{S}$ to be a $2N-2$-dimensional surface which we call the Poincaré section.

While there has been some effort put into studying Poincaré sections in higher dimensions [9] (see references therein), the only ones which can be understood easily and which we use in this thesis are the ones for $N = 2$ (this corresponds to the reduced system in Eq. (1.30)); this gives $\mathcal{S}$ dimension 2 as well.

Definition 3 (Return mapping)**.** *Let $\mathcal{S}$ be the Poincaré section in the phase space of a Hamiltonian system with Hamiltonian $\mathcal{H}$. The return mapping Ω then maps an initial condition on S to the first point where the flow returns to $\mathcal{S}$.*

Such a mapping does not exist everywhere on $\mathcal{S}$, as there are escapes to the event horizon even for $E < 1$ (this is the case which we study). However, there are again many trajectories which do not escape and in this subset of $\mathcal{S}$ the mapping exists.

We can now return to the twist condition in Def. 2. While it requires that its phase space be a cylinder, which will not be our case, as the mapping we will later use acts on a subset of $\mathbb{R}^2$, we can see from the previous section that in the integrable case the motion lies on a nested family of tori where the non-degeneracy condition

$$\det\left(\frac{\partial \omega^\mu}{\partial I_\nu}\right) \neq 0 \tag{1.40}$$

holds, and can be parametrized by action-angle coordinates. In the case of a 4-dimensional phase space of the original Hamiltonian system, the intersection of a torus with a Poincaré section $\mathcal{S}$ is a so-called invariant circle. It has the topology of a circle because of the transversality of the surface of section $\mathcal{Q}$ to the Hamiltonian flow. This allows us to parametrize $\mathcal{S}$ using action-angle coordinates. Such structure remains even in a non-integrable system, giving meaning to the twist condition.

The return mapping Ω on $\mathcal{S}$ is a symplectic twist map. In [10], the symplectic condition is derived in a way that shows that a return mapping is indeed a symplectic map. The twist condition is guaranteed by the definition of action-angle variables [7].

We will now consider the return mapping of a Poincaré section $\mathcal{S}$ for a Hamiltonian system with 2 degrees of freedom. First, let us consider the integrable case. As was already mentioned, the motion lies on a nested family of 2-dimensional tori, so the mapping is represented by a nested family of closed curves called invariant circles. Again, we can parametrize $\mathcal{S}$ by action-angle variables θ and I, in which the map is of the form

$$\Omega : (\theta, I) \mapsto (\theta', I')\,, \tag{1.41a}$$

$$I' = I, \tag{1.41b}$$

$$\theta' = \theta + \omega\,(I)\,. \tag{1.41c}$$

The ω as written here is then called the *rotation number*. It can be determined by using the methods of frequency analysis [11] or by the method of dynamical spectra [12], which we later use in Sec. 1.11.

1.9 KAM theory

Generally, the structure of phase space is altered by perturbing a dynamical system. If we wish to study how a trajectory changes, we need some way to assign a trajectory in the perturbed system to the corresponding trajectory in the unperturbed system; as the structure changes, it is pointless to assign by initial conditions. For example, if we were to take an ϵ-dependent change of variables and apply it together with the variation, such an assignment of trajectories between the original and the perturbed phase space would be ambiguous.

Obviously, a much more sensible way to do this is to use the fundamental frequencies. As can be seen from canonical perturbation theory, if we apply a small perturbation and attempt to solve the Hamilton-Jacobi equation (1.33) perturbatively, we arrive at a series with small denominators of the form $m_1\omega^1 + m_2\omega^2$ summed over $(m_1, m_2) \in \mathbb{Z}^2$, which does not converge, as for any irrational $\omega = \omega^1/\omega^2$ we can find an arbitrarily close rational number. However, there are still ways we can discuss the "measure of irrationality" of a number, which allow us to state when a set of frequencies is far enough from resonances.

Definition 4 (Diophantine numbers [10])**.** *Let $C > 0$ and $q \geq 1$, then we denote*

$$D_q(C) = \{\omega \in \mathbb{R} \setminus \mathbb{Q} : \forall (m,n) \in \mathbb{Z}^2 \setminus \{(0,0)\} \, |n\omega - m| > \frac{C}{n^q}\}. \tag{1.42}$$

We define the set of Diophantine numbers

$$D_q = \bigcup_{C>0} D_q(C). \tag{1.43}$$

Definition 5 (Function norm)**.** *For a j-times differentiable function we define its j-norm as*

$$|f(x,y)|_j = \sup_{m+n\leq j} \left| \frac{\partial^{m+n} f}{\partial x^m \partial y^n} \right|. \tag{1.44}$$

Using this definition, we can now write the KAM theorem as proven by Moser for mappings [10].

Theorem 2 (KAM theorem)**.** *If Ω is a j-times differentiable twist mapping*

$$\frac{\mathrm{d}\Omega}{\mathrm{d}I} \geq K > 0, \tag{1.45}$$

then there is an $\epsilon > 0$ such that all area-preserving maps

$$I'_\mu = I_\mu + f_\mu(I_\nu, \theta^\nu), \tag{1.46a}$$

$$\theta'^\mu = \theta^\mu + \Omega^\mu(I_\nu) + g^\mu(I_\nu, \theta^\nu). \tag{1.46b}$$

with

$$\int_0^{2\pi} f_\mu(I_\nu, \theta^\nu)\, \mathrm{d}\theta^\nu = 0, \tag{1.47a}$$

$$|f|_j + |g|_j < \epsilon K C^2 \tag{1.47b}$$

have rotational invariant circles for all Diophantine frequencies with

$$1 < q < \frac{j-1}{2}. \tag{1.48}$$

These invariant circles are called KAM curves.

The KAM theorem provides the first insight into the typical structure of near-integrable systems. In an integrable system, the mapping consists of a nested family of invariant circles with a fixed point in its center. Upon a small degree of perturbation, some invariant circles remain and so does the fixed point in the center. The set bounded by the outermost of the invariant circles is called the *main island of stability.*

There is a different way to approach the problem of "measure of irrationality" than Diophantine numbers, that is the use of continued fractions. We can express any irrational number in the form of a continued fraction

$$[a_0, a_1, a_2, \ldots] := a_0 + \frac{1}{a_1 + \frac{1}{a_2 + \ldots}}. \tag{1.49}$$

Irrational numbers are harder to approximate by rationals if their continued-fraction-expansion elements are small. An interesting subset is the set of *noble numbers*, which is the set of irrationals for which a positive integer j exists such that $a_i = 1 \quad \forall i \geq j$. The "noblest" of numbers is the *golden mean*

$$\gamma = \frac{1 + \sqrt{5}}{2} = [1, 1, 1, \ldots]. \tag{1.50}$$

Invariant circles with noble rotation numbers typically survive the highest degree of perturbation. Usually, the last invariant circle to be destroyed is the one with $\omega = \gamma - 1 = [0, 1, 1, 1, \ldots]$ as discussed in [12].

1.10 Periodic points, linear stability

An interesting aspect of a symplectic map are periodicity and quasiperiodicity of its orbits. Generally, we call an orbit of a map n-periodic, if n is the lowest integer such that for a point (I, θ) of the orbit

$$\Omega^n (I, \theta) = (I, \theta + 2\pi m), m \in \mathbb{N}. \tag{1.51}$$

If we take the determinant of the symplectic condition in Eq. (1.38), we find that $\det M = \pm 1$. It can be shown [10] that $\det M = 1$ holds, using this, we can study the properties of fixed points and their vicinity. Since M is a real matrix, its characteristic polynomial $\det (M - \lambda I)$ has real coefficients. This means that λ is its root if and only if λ^* (* denotes the complex conjugate number) is its root as well. Also, using the properties of the determinant:

$$0 = \det (J_{2N}) \det (M - \lambda I) = \det \left[\left(M^T \right)^{-1} - \lambda I \right] \det (J_{2N}) = \det \left(M^{-1} - \lambda I \right), \tag{1.52}$$

meaning that λ is a root of the characteristic polynomial if and only if λ^{-1} is as well. Therefore for an eigenvalue λ which is neither real nor on the unit circle λ^{-1}, λ^* and λ^{*-1} are eigenvalues of M as well. This can only occur in four- and higher-dimensional maps. We limit ourselves to two-dimensional maps, where eigenvalues exist in pairs. There are three ways this can happen:

1. $|\lambda_1| = 1, \lambda_1 \notin \mathbb{R} \Rightarrow \lambda_1 = \exp (i\zeta), \lambda_2 = \lambda^{-1} = \lambda^* = \exp (-i\zeta)$: This does not imply the unitarity of M, as the eigenbasis is not necessarily orthogonal

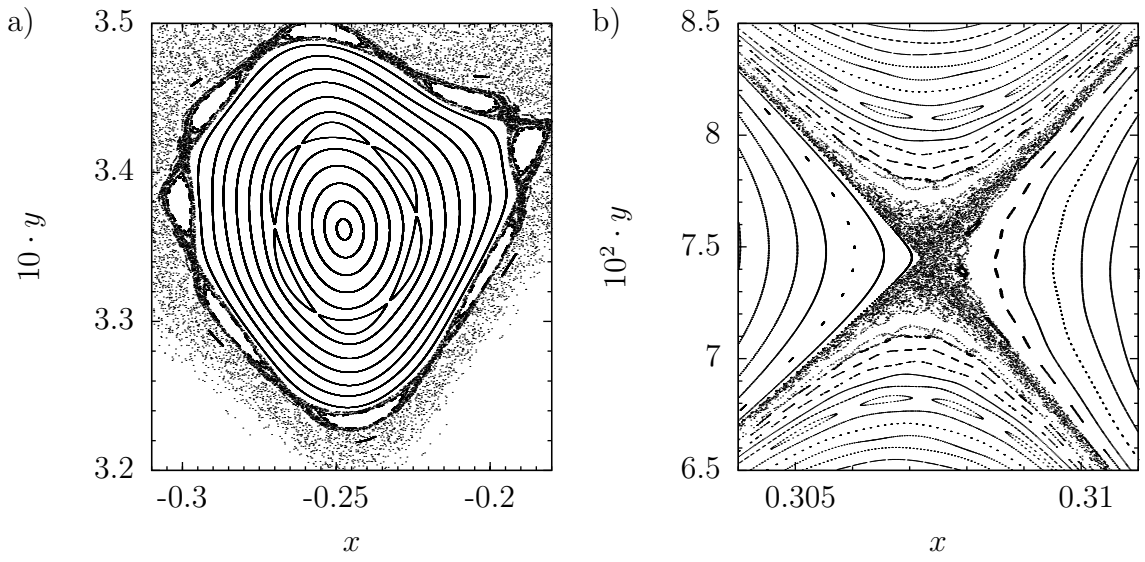

Figure 1.1: a) A typical elliptic periodic point with the island around, b) a typical hyperbolic periodic point with the chaotic zone around.

and the condition $M^\dagger M = MM^\dagger$ is not necessarily met. However, it does cause the eigenvalues of M^n to retain unit absolute value. This is why such a fixed point of M^n is called an elliptic fixed point (or a stable fixed point), as the points in the vicinity of such a point move on an ellipse around the fixed point in the linearized map.

2. $|\lambda_1| \neq 1, \lambda_1 \in \mathbb{R} \Rightarrow \lambda_2 = \lambda^{-1}$: This causes points in the vicinity of the fixed point move on a hyperbole in the linearized map except for points in one of the eigendirections of M, therefore this point is called a hyperbolic point (or an unstable fixed point).

3. $\lambda_1 = \lambda_2 = \pm 1$: Such a point is called indifferently stable.

The KAM theorem gives stability for circles of Diophantine frequencies. It does not, however, state, what happens to those with rational frequencies. The Poincaré-Birkhoff theorem gives an insight into the behavior of periodic orbits after perturbation.

Theorem 3 (Poincaré-Birkhoff theorem [7])**.** *For a curve of rational rotation number r/s ($r, s \in \mathbb{N}$ incommensurable) of an unperturbed twist mapping, there exists $k \in \mathbb{N}$ such that $2ks$ periodic points of period s remain after the perturbation. These periodic points are alternately stable and unstable.*

Corollary. Typically $k = 1$.

In an integrable system, a single resonant torus provides an infinite number of different periodic trajectories; the perturbation reduces them to a finite number, half of which are stable and the other half unstable. Around the stable periodic points of the mapping arise smaller islands of stability. As the structure of the phase space is self-similar, the same applies to the mapping Ω^s around these points, giving rise to higher-order resonances. A wonderful example of this self-similar structure is shown for the standard map in Fig. 1.2.

In the rest of this section we will denote points in $\mathcal{S}$ by $\mathbf{x}$ for practical reasons.

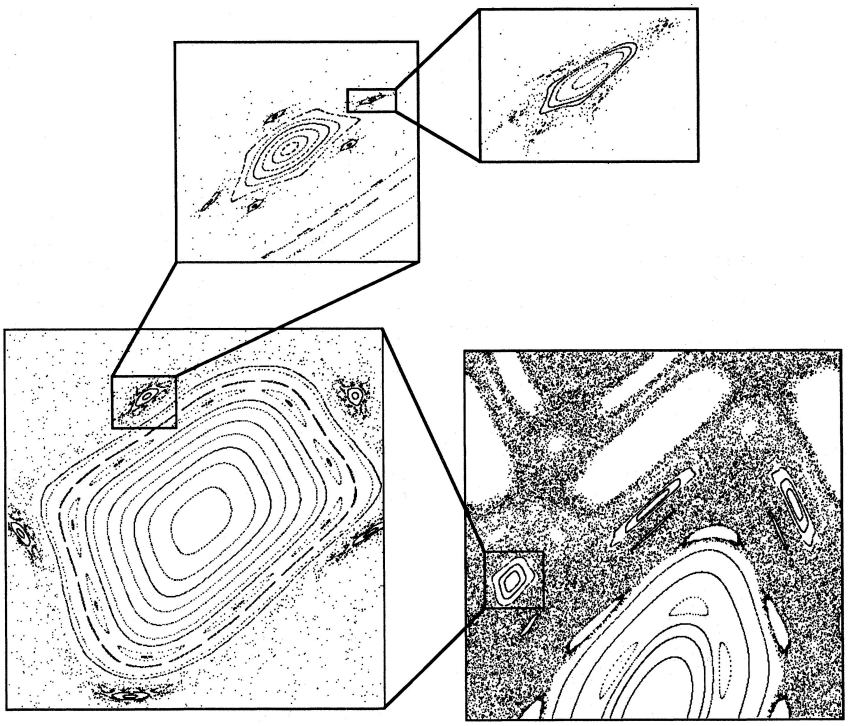

Figure 1.2: Example of the self-similar structure taken from [10], plotted using the standard map.

Theorem 4 (Stable manifold theorem [13])**.** *Let Ω be a symplectic mapping on $\mathcal{S}$ and $\mathbf{x}^f$ its fixed point. Then there exists a smooth manifold $W^s\left(\mathbf{x}^f\right)$ called the stable manifold and a smooth manifold $W^u\left(\mathbf{x}^f\right)$ called the unstable manifold defined as*

$$W^s\left(\mathbf{x}^f\right) = \{\mathbf{x} \in \mathcal{S} : \Omega^j \mathbf{x} \overset{j\to\infty}{\longrightarrow} \mathbf{x}^f\}, \tag{1.53a}$$

$$W^u\left(\mathbf{x}^f\right) = \{\mathbf{x} \in \mathcal{S} : \Omega^{-j} \mathbf{x} \overset{j\to\infty}{\longrightarrow} \mathbf{x}^f\}. \tag{1.53b}$$

Corollary. An important property of these manifolds is their invariance, meaning that

$$\Omega W^s\left(\mathbf{x}^f\right) = W^s\left(\mathbf{x}^f\right), \tag{1.54a}$$

$$\Omega W^u\left(\mathbf{x}^f\right) = W^u\left(\mathbf{x}^f\right). \tag{1.54b}$$

Theorem 5 (Hartman-Grobman theorem [14])**.** *The behavior of $W^s\left(\mathbf{x}^f\right)$ and $W^u\left(\mathbf{x}^f\right)$ around $\mathbf{x}^f$ is topologically equivalent to the monodromy matrix M.*

We can now study the properties of the manifolds $W^u\left(\mathbf{x}^f\right)$ and $W^s\left(\mathbf{x}^f\right)$. It can be easily seen that for any two hyperbolic fixed points $\mathbf{x}_1^f \neq \mathbf{x}_2^f$

$$W^u\left(\mathbf{x}_1^f\right) \bigcap W^u\left(\mathbf{x}_2^f\right) = \emptyset, \tag{1.55a}$$

$$W^s\left(\mathbf{x}_1^f\right) \bigcap W^s\left(\mathbf{x}_2^f\right) = \emptyset. \tag{1.55b}$$

This is obvious, if there existed a point x that belonged to two different stable manifolds, the limit of $\Omega^j x$ as $j \to \infty$ would be both $\mathbf{x}_1^f$ and $\mathbf{x}_2^f$; the argument

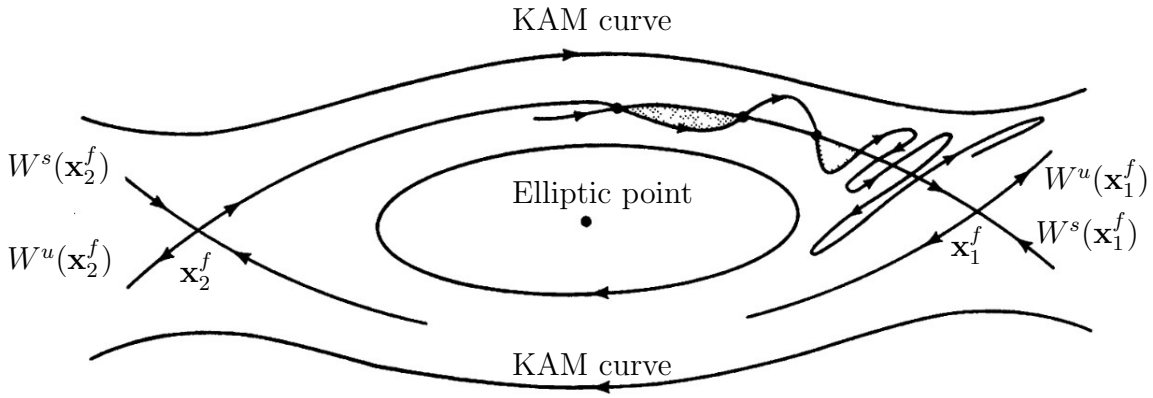

Figure 1.3: The typical phase space structure, figure taken from [7].

for unstable manifolds is the same with $\Omega^{-j}x$. Also, neither of the manifolds can cross itself, as this would result in the existence of a periodic point on the manifold. However, points where $W^u\left(\mathbf{x}_1^f\right)$ crosses $W^s\left(\mathbf{x}_2^f\right)$ can exist, and then, in the case that $\mathbf{x}_1^f = \mathbf{x}_2^f$, the point is called *homoclinic*; if $\mathbf{x}_1^f \neq \mathbf{x}_2^f$, the point is called *heteroclinic*. If there exists a single homoclinic point (except for $\mathbf{x}_1^f = \mathbf{x}_2^f$), then applying Ω^n for any $n \in \mathbb{Z}$ generates infinitely many homoclinic points, as both the stable and the unstable manifold are invariant. These points generically exist and an orbit passing through such a point x then must fulfill $\Omega^j x \to \mathbf{x}_1^f$ for both $j \to \infty$ and $j \to -\infty$. The topology of such an orbit is different from that of a KAM curve. This typical structure is shown in Fig. 1.3.

The self-similar structure of a mapping means that if we take a hyperbolic point, we find higher-order resonances around the neighboring islands, these once again have their own hyperbolic points with their own unstable and stable manifolds. This typically leads to the existence of heteroclinic points as well; the existence of one again implies the existence of infinitely many, the argument is the same as with homoclinic points. This behavior is what gives rise to the extremely complicated dynamics near hyperbolic points. As can be seen in Fig. 1.1 b), orbits near a hyperbolic point then typically densely fill the area around the resonance.

1.11 Dynamical spectra

Angular dynamical spectra are a method of analysis of dynamical systems with discrete time evolution, the method is described in [12].

We consider a two-dimensional symplectic map Ω, in our case the return mapping of the Poincaré section $\mathcal{S}$. Points in $\mathcal{S}$ are defined by two parameters x and y. Let the initial point of an orbit be (x_i, y_i) and then the successive points $(x_n, y_n) := \Omega^n (x_i, y_i)$ for $n \in \mathbb{N}$. Also, let (x_c, y_c) be a fixed point of Ω lying at the center of the main island of stability. We can then simply define *rotation angles*

$$\vartheta_n := \operatorname{ang}\left[(x_{n+1} - x_c, y_{n+1} - y_c), (x_n - x_c, y_n - y_c)\right]. \tag{1.56}$$

It is the angle between the vectors from the point (x_c, y_c) to two successive points of the orbit. It is a matter of convention to define the interval in which the angles lie, we take $[0, 2\pi)$.

We define the spectrum of rotation angles as the distribution of these angles

$$S(\vartheta) := \frac{dN(\vartheta)}{Nd\vartheta}. \tag{1.57}$$

This spectrum has an invariant character along the same orbit/within the same chaotic zone. We can therefore define the first angular moment

$$\nu_\vartheta := \frac{1}{2\pi} \int_0^{2\pi} S(\vartheta)\, \mathrm{d}\vartheta. \tag{1.58}$$

The simplest way to calculate the angular moments numerically while evolving an orbit is to calculate the rotation angles and calculate their average

$$\nu_\vartheta = \lim_{N\to\infty} \frac{1}{2\pi N} \sum_{j=1}^{N} \vartheta_j. \tag{1.59}$$

It can be easily seen that the right side does converge to the angular moment and that it corresponds to the rotation number ω as used in Eqs. (1.41).

A way to analyze the system is to take a set of initial conditions along a curve in the Poincaré section and to calculate the angular moments for these orbits. If we then plot the angular moments as a function of a parameter to determine the initial condition (we call this the rotation curve), we can see some of the properties of the system. Most importantly, in an integrable system, if the curve is chosen such that it crosses every invariant circle only once, then the rotation curve is monotone, namely growing in the direction from the center outwards, thanks to the twist condition. In the case of a near-integrable system with the standard behavior such as islands of stability and chaotic zones, the behavior of the rotation curve changes significantly. The rotation curve has a plateau where it crosses an island of stability; this behavior differs from that of KAM curves because of our choice of x_c and y_c in the center of the main island of stability. This allows us to detect even small islands by studying the rotation curve. On the other hand, while crossing a chaotic zone, the rotation curve no longer exhibits monotone behavior, which allows us to detect even thin chaotic zones. This behavior is again described in [11], [12].

1.12 Chaos

Definition 6 (Devaney's definition of chaos)**.** *By Devaney's definition [15] we call a symplectic map Ω on a compact metric space $(\mathcal{S}, \rho)$ chaotic, if:*

1. *It is topologically transitive:*
   For any two non-empty open $U_1, U_2 \subset \mathcal{S}$ there exists a $n \in \mathbb{N}$ such that

   $$(\Omega^n U_1) \cap U_2 \neq \emptyset. \tag{1.60}$$

2. *Its periodic points are dense in the phase space.*

3. *It is sensitive to initial conditions:*
   There exists a $\delta > 0$ such that for every point $x \in \mathcal{S}$ and every neighborhood $U(x)$ there exist $y \in U(x)$ and $n \in \mathbb{N}$ such that $\rho(\Omega^n x, \Omega^n y) > \delta$.

Corollary. It has been shown by Banks et al. in [16] that 1. and 2. $\Rightarrow$ 3., meaning that we only need topological transitivity and denseness of periodic points for the system to exhibit sensitivity to initial conditions.

1.13 Deviation vector

Definition 7. *We denote $T_{(q^\mu,p_\mu)}\mathcal{X}$ the tangent space of the phase space $\mathcal{X}$ in the point (q^μ, p_μ). The tangent bundle*

$$T\mathcal{X} := \bigcup_{(x^\mu,p_\mu)\in\mathcal{X}} T_{(x^\mu,p_\mu)}\mathcal{X}. \tag{1.61}$$

The deviation vector is a point $(\xi^\mu, \psi_\mu) \in T\mathcal{X}$.

Such a deviaton vector can be interpreted as the difference of two nearby points in the phase space. Such a deviation vector then evolves by the variational equations, which we obtain by expanding the equations of motion for the system in the state $x^\mu + \gamma\xi^\mu$, $p_\mu + \gamma\psi_\mu$ in γ and taking the terms only to first-order in γ. For the geodesic deviation equation, it is simpler to use the typical form of the geodesic equation

$$\ddot{x}^\mu + \Gamma^\mu{}_{\kappa\lambda}\dot{x}^\kappa\dot{x}^\lambda = 0. \tag{1.62}$$

Taking the equation for the deviating trajectory we get

$$\ddot{x}^\mu + \gamma\ddot{\xi}^\mu + \Gamma^\mu{}_{\kappa\lambda}\left(x^\mu + \gamma\xi^\mu\right)\left(\dot{x}^\kappa + \gamma\dot{\xi}^\kappa\right)\left(\dot{x}^\lambda + \gamma\dot{\xi}^\lambda\right) = 0. \tag{1.63}$$

By expanding this equation to first order in γ, we gain an equation whose terms constant in γ are the geodesic equation itself and the ones linear in γ give the geodesic deviation equation in the form

$$\ddot{\xi}^\mu + \frac{\partial\Gamma^\mu{}_{\kappa\lambda}}{\partial x^\nu}\dot{x}^\kappa\dot{x}^\lambda\xi^\nu + 2\Gamma^\mu{}_{\kappa\lambda}\dot{x}^\kappa\dot{\xi}^\lambda = 0. \tag{1.64}$$

We want to discern chaotic from regular behavior by measuring the growth of deviation vectors. We first need to define a measure of deviation vectors invariant under coordinate transformation. In [17] the choice

$$\Xi^2 = g_{\mu\nu}\xi^\mu\xi^\nu + g_{\mu\nu}\frac{\mathrm{D}\xi^\mu}{\mathrm{d}\tau}\frac{\mathrm{D}\xi^\nu}{\mathrm{d}\tau} \tag{1.65}$$

is suggested as it measures the deviation in the phase space. We will, however, use the simpler choice [17]

$$\Xi^2 = g_{\mu\nu}\xi^\mu\xi^\nu \tag{1.66}$$

which only measures the deviation in the configuration space and is simpler to implement.

For chaotic orbits, the growth of deviation vectors is typically exponential, of the form ($\lambda > 0$)

$$\Xi(\tau) \sim \exp(\lambda\tau). \tag{1.67}$$

For unstable periodic orbits (corresponding to hyperbolic points of the return mapping) this is obvious. For non-periodic chaotic orbits a periodic orbit of

arbitrarily large period can be found arbitrarily close [7]. We therefore study the convergence of the finite maximal Lyapunov characteristic exponent

$$\mathrm{FmLCE}\,(\tau) := \frac{1}{\tau} \log \frac{\Xi\,(\tau)}{\Xi\,(0)}. \tag{1.68}$$

This indicator clearly converges to λ if Eq. (1.67) holds for large values of τ.

For regular orbits the growth of Ξ is typically linear. This can be easily seen using action-angle variables, as the evolution of the system is then linear as well. We would like to see how the FmLCE defined in the previous paragraph behaves in this case. If the measure of the deviation vector is of the form

$$\Xi\,(\tau) = \Xi\,(0)\,(1 + A\tau)\,, \tag{1.69}$$

then $\mathrm{FmLCE}\,(\tau)$ apparently converges to zero for $\tau \to \infty$. If plotted in logarithmic scale (in both τ and FmLCE), for large enough values of τ

$$\mathrm{FmLCE}\,(\tau) \sim \frac{1}{\tau}. \tag{1.70}$$

Then we see a straight line with slope -1 converging to zero, while for a chaotic orbit $\mathrm{FmLCE}\,(\tau)$ converges to the maximal Lyapunov exponent

$$\mathrm{mLCE} := \lim_{\tau \to \infty} \mathrm{FmLCE}\,(\tau) > 0. \tag{1.71}$$

This is a way to discern chaotic from regular orbits. Its greatest problem is that until we see the FmLCE converge to a non-zero value we cannot state categorically whether the trajectory is regular or chaotic. We call the time it takes for FmLCE to display the behavior we expect from chaotic trajectories the Lyapunov time. It is a good rule of thumb that its value is approximately 1/mLCE.

2. Numerical results

2.1 Effective potential

First of all, we call the subset $\theta = \pi/2$ of the spacetime manifold the equatorial plane. It is noteworthy that while we use the word "plane", its geometry is different from that of a plane. It does, however, possess properties which are interesting both in relation to the spacetime properties (reflection symmetry of the spacetime) and in relation to the set of Boyer-Lindquist-like coordinates t, r, θ, ϕ.

It is necessary to discuss the values of the metric parameters we will be studying. To work in dimensionless units, we set the scale of all the parameters with respect to M, which practically is equivalent to setting $M = 1$. The value of the spin a can then be chosen anywhere in the interval $[-1, 1]$. Setting it equal to ± 1 would cause the object to become an extremal black hole. As can be seen in [1], this would severely limit our ability to vary the parameter ϵ_3, which would be limited to non-positive numbers in order to avoid pathologies, namely a disjoint event horizon as described in [3]. We will therefore work with a value lower than $a = 1$.

The value $a = 0$ is an uninteresting case, as this would simplify the metric to

$$\mathrm{d}s^2 = g_{tt}(r)\,\mathrm{d}t^2 + g_{rr}(r)\,\mathrm{d}r^2 + r^2\left(\mathrm{d}\theta^2 + \sin^2\theta \mathrm{d}\phi^2\right). \tag{2.1}$$

This form of the metric describes a spherically symmetric spacetime. In such a spacetime for any geodesic trajectory there exists a change of coordinates which doesn't affect the metric and moves the trajectory to the equatorial plane, making such motion fully integrable and possible to investigate using the methods shown later in this section. Another way to view the integrability issue is that there is an additional constant of the motion, that is a second component of the angular momentum (L_x and L_y are in involution with L_z), causing the motion to be integrable.

Last of all, setting $a < 0$ would only change the sign of $g_{t\phi}$, meaning that using the transformation $\phi \mapsto -\phi$, we would get the same spacetime except for a, which would again change sign. We can therefore limit our choice to $a \in (0, 1)$.

As we know the Hamiltonian (1.30) to be not only an integral of the motion, but to be the same for every orbit, we can write

$$(p_r)^2 + \frac{g_{rr}}{g_{\theta\theta}}(p_\theta)^2 = -g_{rr}\left(1 + \frac{g_{\phi\phi}E^2 + g_{tt}L_z^2 + 2g_{t\phi}EL_z}{g_{tt}g_{\phi\phi} - g_{t\phi}^2}\right). \tag{2.2}$$

The functions g_{rr} and $g_{\theta\theta}$ are positive everywhere above the event horizon (the set where g_{rr} diverges), which is our area of interest. For a particle with the energy E and z-component of angular momentum L_z then the right side of this equation must be non-negative, which determines the region, in which such a particle moves. We denote the *effective potential*

$$V_{\text{eff}} := g_{rr}\left(1 + \frac{g_{\phi\phi}E^2 + g_{tt}L_z^2 + 2g_{t\phi}EL_z}{g_{tt}g_{\phi\phi} - g_{t\phi}^2}\right). \tag{2.3}$$

The first use of the effective potential is to determine the characteristics of an orbit lying in the equatorial plane. These orbits do exist, because the spacetime is reflection symmetric, so orbits with initial conditions $\theta = \pi/2$, $p_\theta = 0$ remain in the equatorial plane. A particle then moves in the region where $V_{\text{eff}}(r, \pi/2) \leq 0$. The usual shape of the effective potential is as shown in Fig. 2.1. In the case a) the particle's r coordinate oscillates between the two roots of the effective potential. In the case b) the particle plunges into the central object. These two trajectories are plotted in the equatorial plane in Fig. 2.1 c) and d). As the equatorial plane is parametrized by polar-like coordinates r and ϕ, the plots are made using Cartesian-like coordinates $r\cos\phi$ and $r\sin\phi$. The initial conditions for these trajectories were chosen $r = 5$, $p_r > 0$. The roots of the effective potential $V_{\text{eff}}(r, \pi/2)$, i.e. the turning points, are plotted as red circles to illustrate the properties of trajectories in the equatorial plane. The black hole's horizon is plotted green.

Trajectories lying in the equatorial plane are always regular, as the coordinate $\theta = \pi/2$ remains constant during the motion and so does $p_\theta = 0$, so the motion of the reduced system now lies in a two-dimensional subset of the phase space with a non-trivial integral $\mathcal{H}$.

In the case of trajectories which do not lie in the equatorial plane Eq. (2.2) holds as well, the difference is that p_θ is no longer identically zero. We define the *curve of zero velocity* (CZV) as $V_{\text{eff}}(r, \theta) = 0$; as the left side of Eq. (2.2) is non-negative above the horizon, the CZV is the boundary of the accessible zone in the (r, θ) plane. The plane $\phi = \text{const}$, for simplicity $\phi = 0$, in the non-reduced system is called the *meridian plane*, in which r and θ are again polar-like coordinates, it is therefore geometrically more accurate to display it using coordinates $(r\sin\theta, r\cos\theta)$. In Fig. 2.2 the CZV is shown with the same parameters as the effective potential in Fig. 2.1. In a) and b), the bounded case is shown, in c) and d) the case allowing plunging orbits is shown. Several trajectories of the system are plotted in Fig. 2.2.

2.2 Surface of section

We study the dynamics of the reduced system of Eq. (1.30) by using a surface of section. As we have described in Sec. 1.8, we define $\mathcal{Q}$ as the set of points in the reduced system's phase space for which $\theta = \pi/2$ and $p_\theta > 0$ hold; $\mathcal{E}$ as the set of points for which $\mathcal{H} = -1/2$ holds. In order to study the return mapping, we need to parametrize the surface $\mathcal{S} = \mathcal{Q} \cap \mathcal{E}$. This indeed is a two-dimensional surface. We parametrize it using coordinates r, p_r, as is typical, see e.g. [17], [18]

We have to verify that these coordinates uniquely determine the point in phase space. Using the definition of $\mathcal{Q}$, we see that $\theta = \pi/2$ is as well uniquely defined. As for p_θ, its absolute value is determined by the definition of $\mathcal{E}$. In the case that it is positive, the definition of $\mathcal{Q}$ determines that the point is the one with $p_\theta > 0$. The points in $\mathcal{S}$ are subject to the condition (2.2), therefore

$$|p_r| < \sqrt{-V_{\text{eff}}(r, \pi/2)}. \tag{2.4}$$

This condition gives the ranges of values of the parameters r and p_r which fully parametrize $\mathcal{S}$.

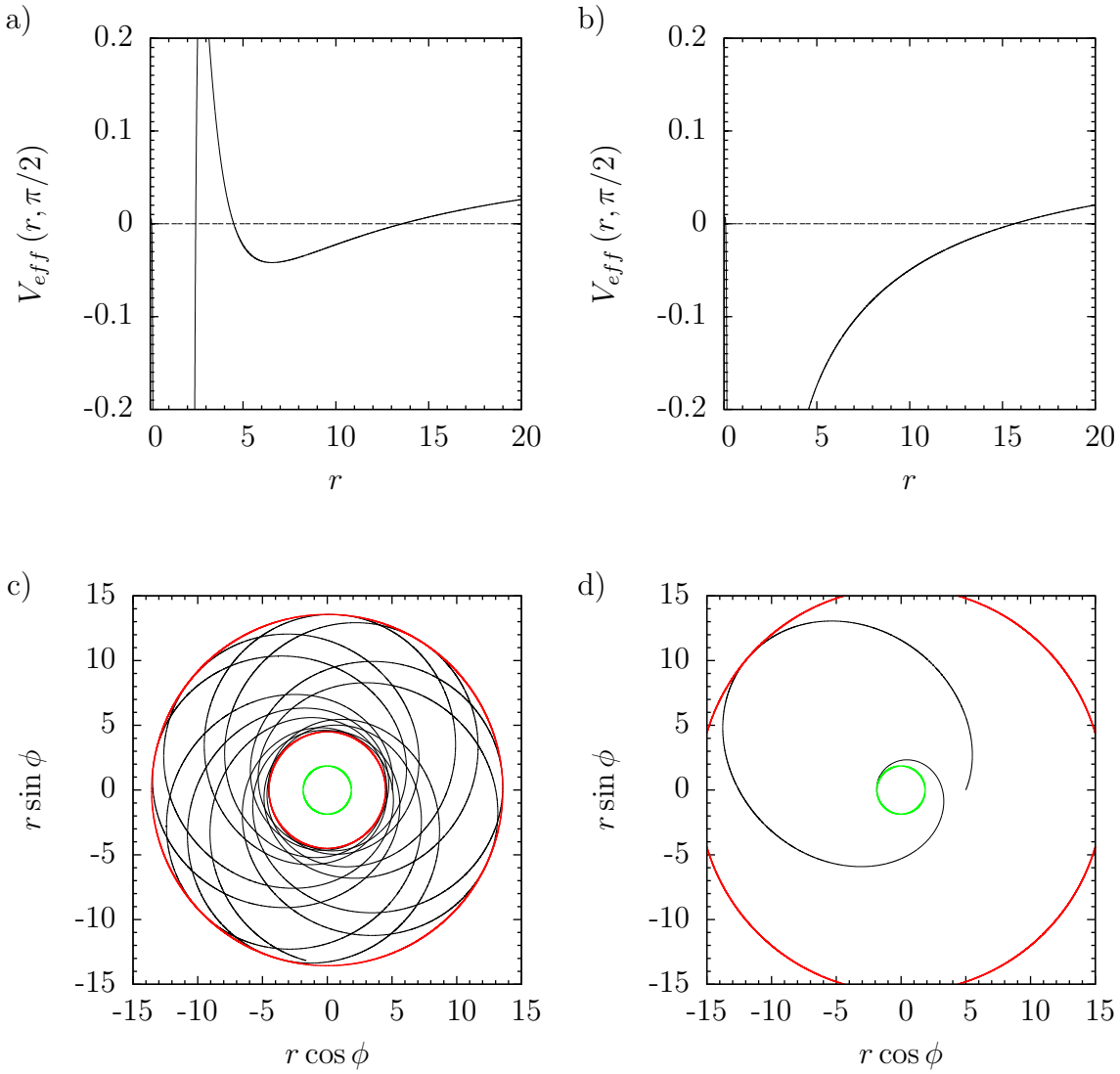

Figure 2.1: a) the effective potential for a quasiperiodic orbit, $L_z = 3.20$, b) the effective potential allowing plunging orbits, $L_z = 2.85$, c) the trajectory corresponding to (a), d) the trajectory corresponding to (b); parameters taken $M = 1$, $a = 0.5$, $\epsilon_3 = 0.3$, $E = 0.95$.

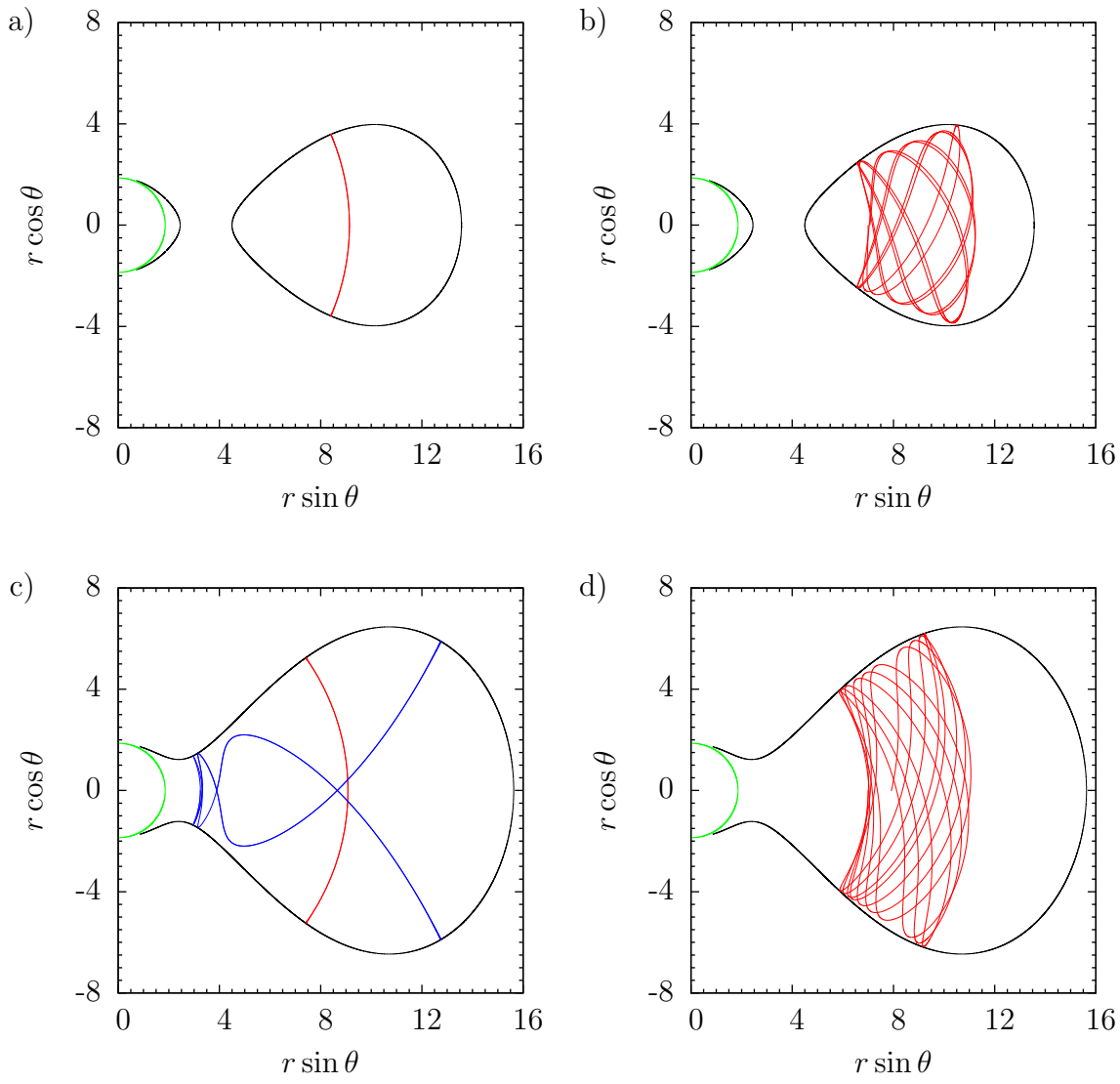

Figure 2.2: Projections of trajectories on the meridian plane bounded by the CZV (black) and the horizon (green), a) the period-1 orbit (red) for $L_z = 3.20$; b) a KAM orbit (red) for $L_z = 3.20$; c) the period-1 orbit (red), the 5/7 periodic orbit (blue) for $L_z = 2.85$; d) a KAM orbit (red) for $L_z = 2.85$; parameters taken $a = 0.5$, $\epsilon_3 = 0.3$, $E = 0.95$.

The points in $\mathcal{S}$ for which

$$|p_r| = \sqrt{-V_{\text{eff}}\left(r, \pi/2\right)} \tag{2.5}$$

holds form a curve in the boundary of $\mathcal{S}$. This curve is the boundary of $\mathcal{S}$ in the (r, p_r) plane. It corresponds to points of $\mathcal{Q}$ for which $p_\theta = 0$, meaning that points on the boundary curve correspond to orbits in the equatorial plane. However, they are not, strictly speaking, points in $\mathcal{S}$, as its definition requires that $p_\theta > 0$; any trajectory which in at least one point has $\theta = \pi/2$ and $p_\theta = 0$ necessarily lies in the equatorial plane because of the spacetime's reflection symmetry, therefore extending the definition of $\mathcal{Q}$ to $p_\theta \geq 0$ would violate the transversality condition.

The properties of the boundary curve are easily shown using the properties of the effective potential: the set of values r for which the effective potential restricted to the equatorial plane $V_{\text{eff}}\left(r, \pi/2\right)$ is negative typically has 1 or 2 maximal connected components as seen in Fig. 2.1, the boundary curve then also divides $\mathcal{S}$ into 1 or 2 accessible zones in the (r, p_r) plane.

Figure 2.3 shows the phase portrait of the return mapping for both the integrable case $\epsilon_3 = 0$ and for the perturbed case $\epsilon_3 = 0.3$. For a) and b), the boundary expressed by (2.5) is plotted as well with a dashed line. No visible signs of chaos can be seen. However, in c) and d), a close-up of the left tip of the main island of stability is shown and more significant differences arise. We can see that in c) there are still only invariant curves, as it is a surface calculated for the Kerr metric, while d) shows several resonances and chaotic trajectories outside and inside the island.

In systems with escapes chaos is more prominent than in others because of the appearance of an unstable point. We, therefore, take the parameters which allow us to get trajectories which eventually plunge in the central object. We take $a = 0.5$, $E = 0.95$ and $L_z = 2.85$. The left tips of the surfaces of section for ϵ_3 from -0.7 to 0.7 with intervals of 0.1 (except for 0, which is integrable) have been calculated with $N = 3000$ points per initial condition and are shown in Figs. 2.4-2.17 in the order of ϵ_3: $0.1 \to 0.7$, then $-0.1 \to -0.7$. Initial conditions were taken along the $p_r = 0$ line with initial values of r taken in intervals of 0.0002. They are plotted together with the corresponding rotation curves, which have been calculated with $N = 4096$ points per initial condition and whose initial conditions were taken along the $p_r = 0$ line with initial values of r taken in intervals of 0.00005.

The surfaces of section shown along with the rotation curves display the typical behavior of the rotation curve. For example, if we look at Fig. 2.6, we see the non-monotonic variations where passing through the chaotic sea and the dive where passing through a hyperbolic fixed point at the 3/4 resonance. The behavior within a resonance is best seen in the case of $\epsilon_3 < 0$, for example Fig. 2.14 shows a large plateu of the 3/4 resonance.

It is interesting to note the behavior of three significant resonances, which are plotted in colors in the surfaces of section: 3/4 (plotted in red), 19/25 (plotted in green) and 13/17 (plotted in blue). We see in Figs. 2.6, 2.14 that for positive values of ϵ_3 the fixed point lying on the horizontal line $p_r = 0$ is hyperbolic for the resonance 3/4 and elliptic for 19/25, while for negative values of ϵ_3 these two resonances "switch roles". To even further demonstrate the complexity of the perturbation, we see that the resonance 13/17 does not exhibit this behavior, as

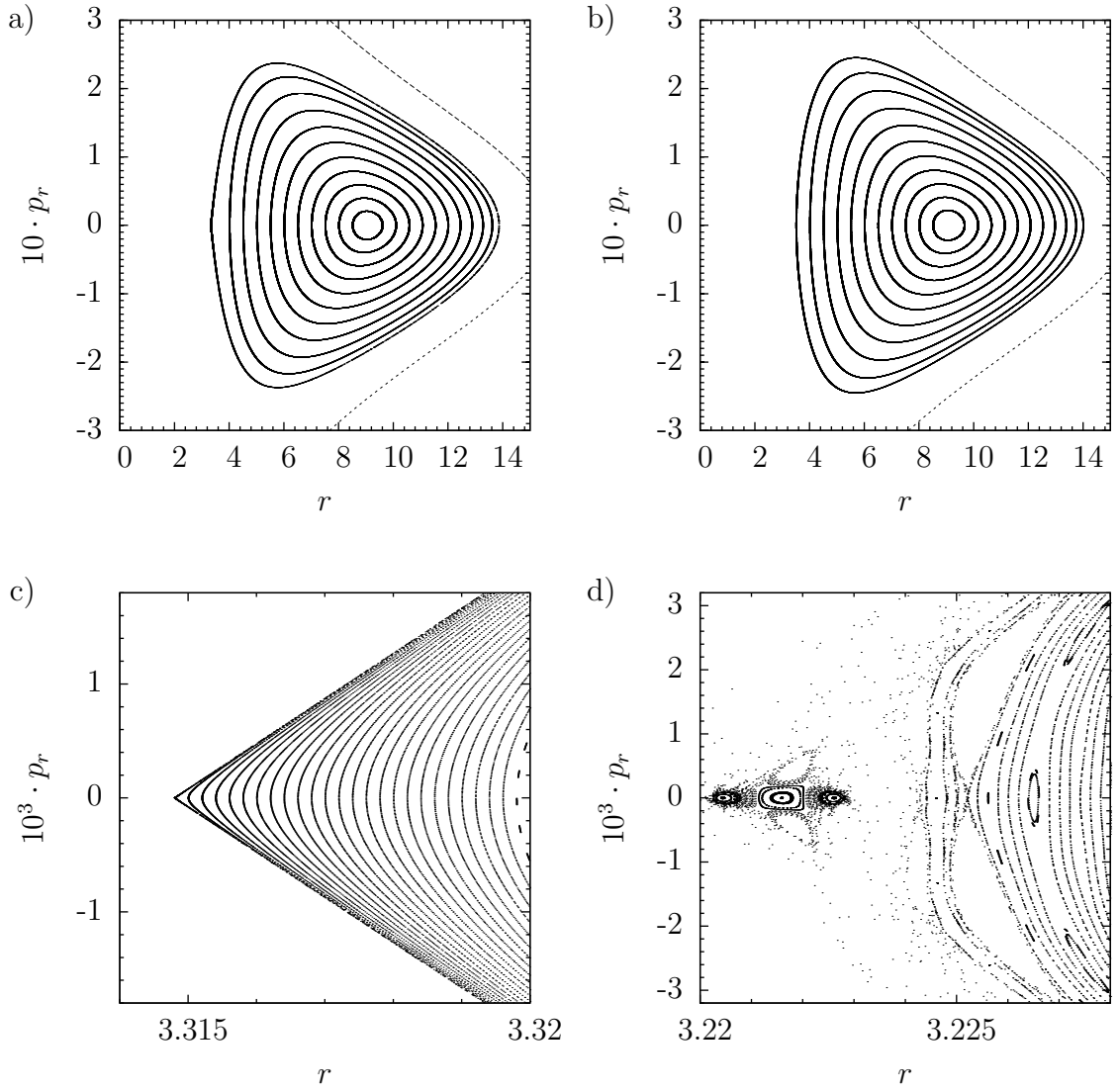

Figure 2.3: Surfaces of section: a) integrable (Kerr) metric ($\epsilon_3 = 0$), b) perturbed metric ($\epsilon_3 = 0.3$), c) detail of the left tip of the main island of stability of (a), d) detail of the left tip of the main island of stability of (b); parameters taken: $a = 0.5$, $E = 0.95$, $L_z = 2.85$.

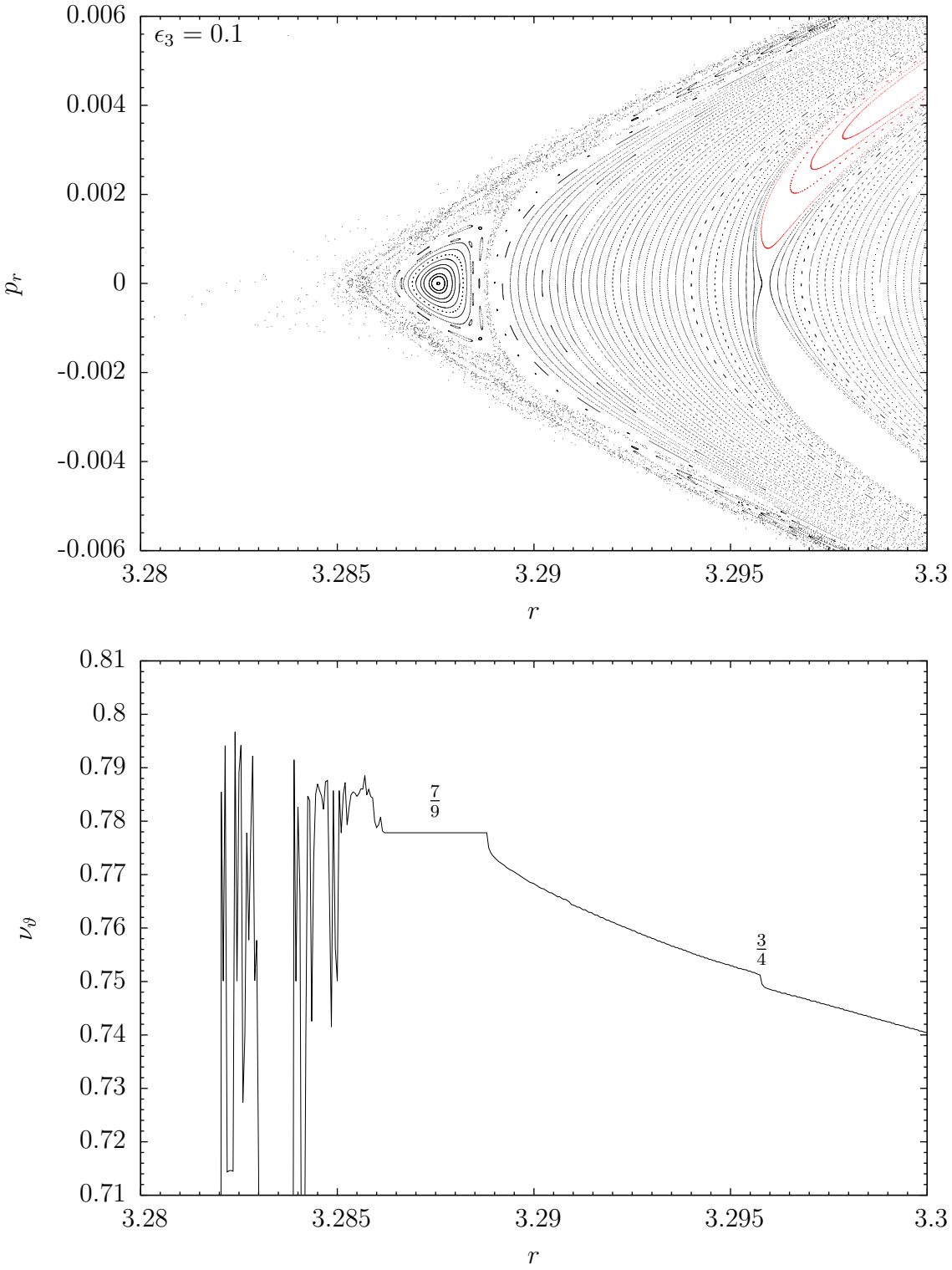

Figure 2.4: Left tip of the surface of section for $\epsilon_3 = 0.1$ with the corresponding rotation curve and fractions denoting resonances; parameters taken: $a = 0.5$, $E = 0.95$, $L_z = 2.85$.

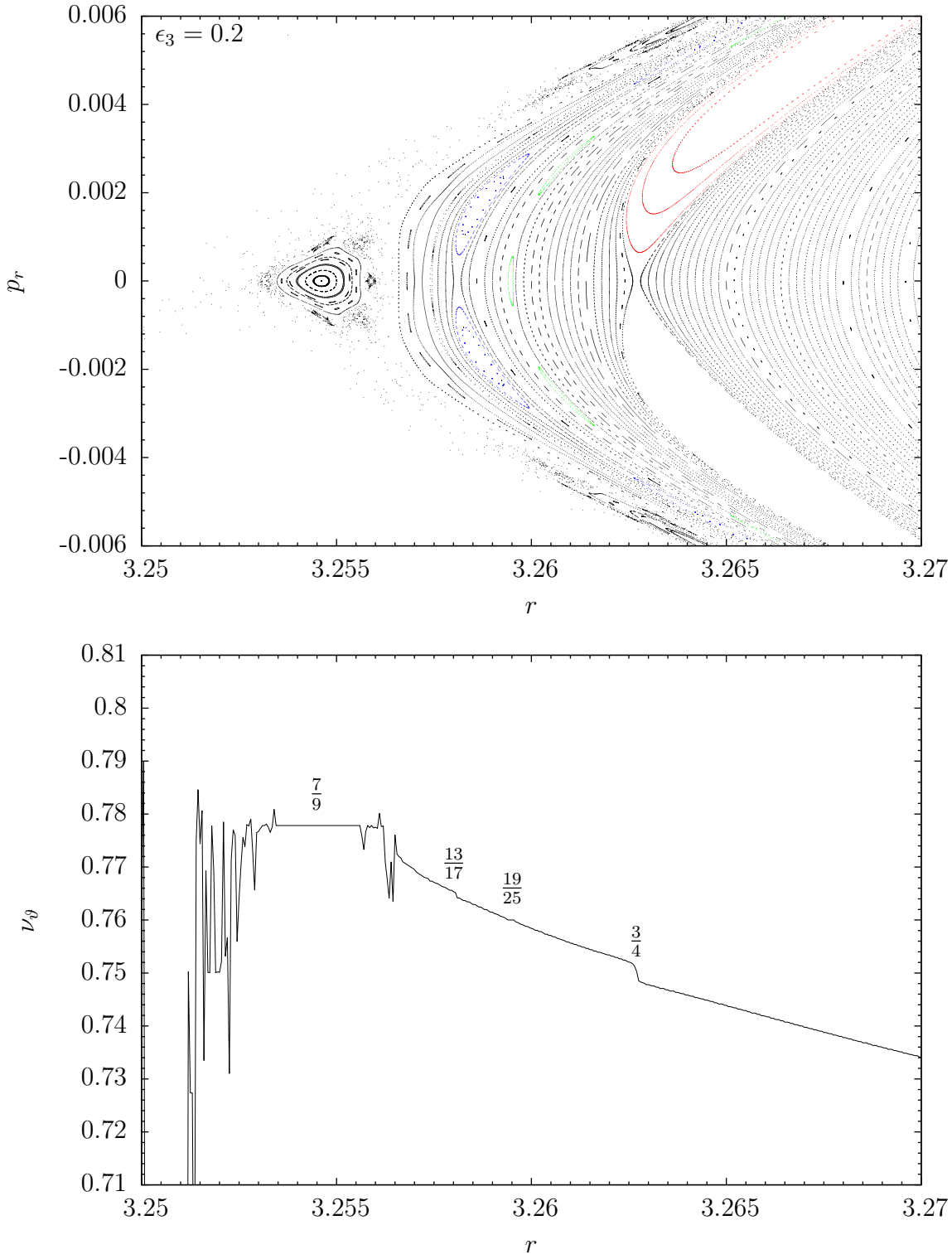

Figure 2.5: Left tip of the surface of section for $\epsilon_3 = 0.2$ with the corresponding rotation curve and fractions denoting resonances; parameters taken: $a = 0.5$, $E = 0.95$, $L_z = 2.85$.

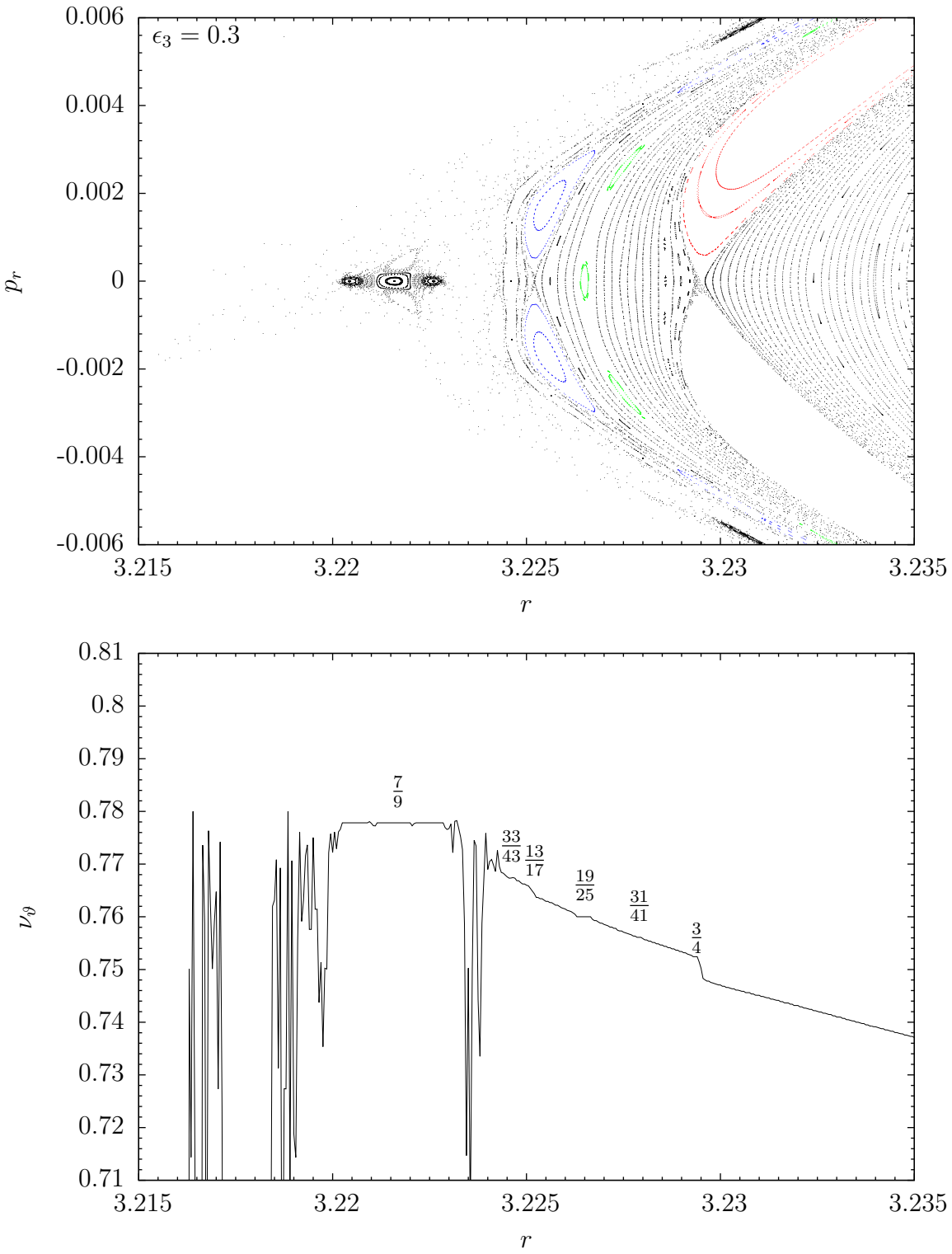

Figure 2.6: Left tip of the surface of section for $\epsilon_3 = 0.3$ with the corresponding rotation curve and fractions denoting resonances; parameters taken: $a = 0.5$, $E = 0.95$, $L_z = 2.85$.

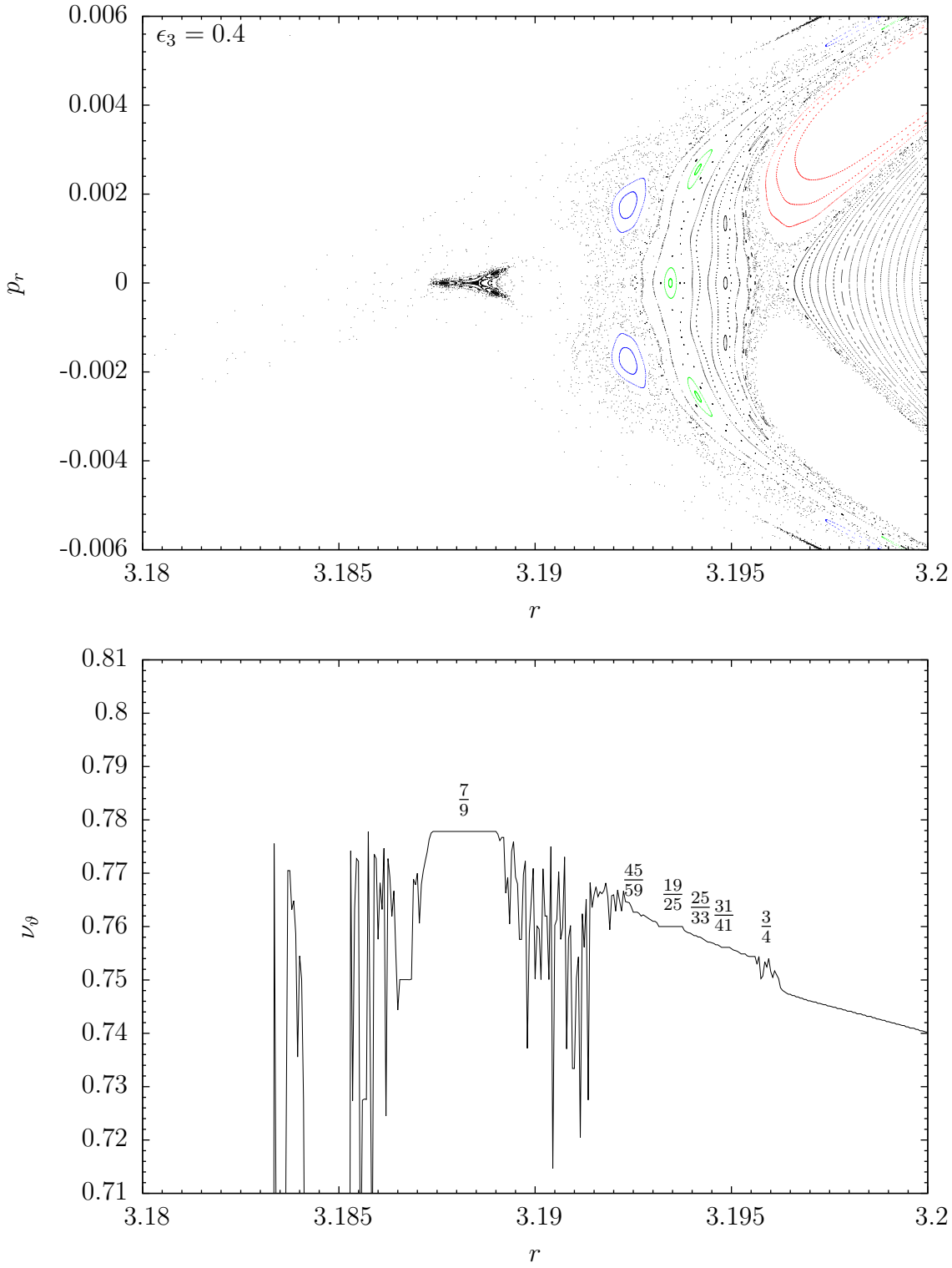

Figure 2.7: Left tip of the surface of section for $\epsilon_3 = 0.4$ with the corresponding rotation curve and fractions denoting resonances; parameters taken: $a = 0.5$, $E = 0.95$, $L_z = 2.85$.

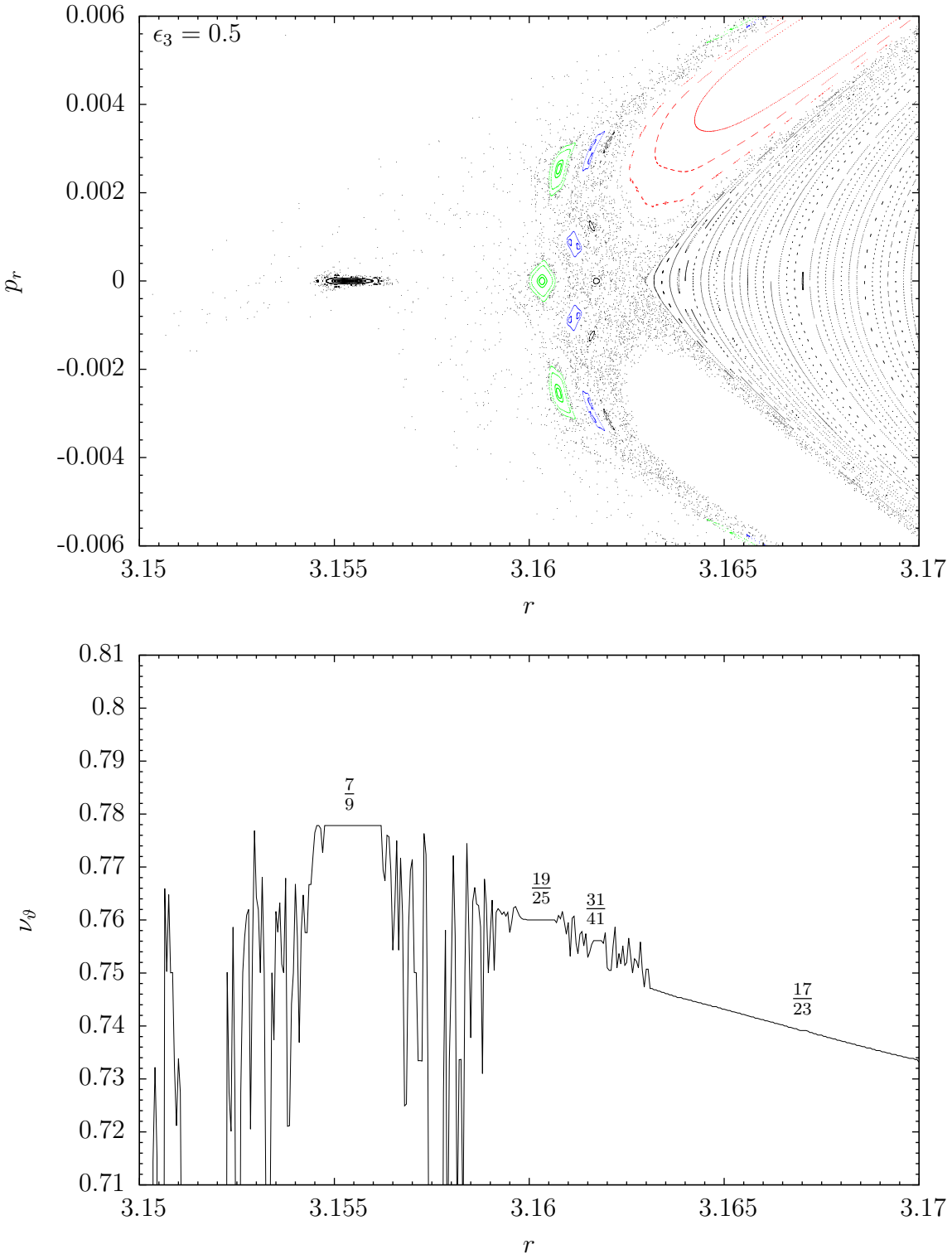

Figure 2.8: Left tip of the surface of section for $\epsilon_3 = 0.5$ with the corresponding rotation curve and fractions denoting resonances; parameters taken: $a = 0.5$, $E = 0.95$, $L_z = 2.85$.

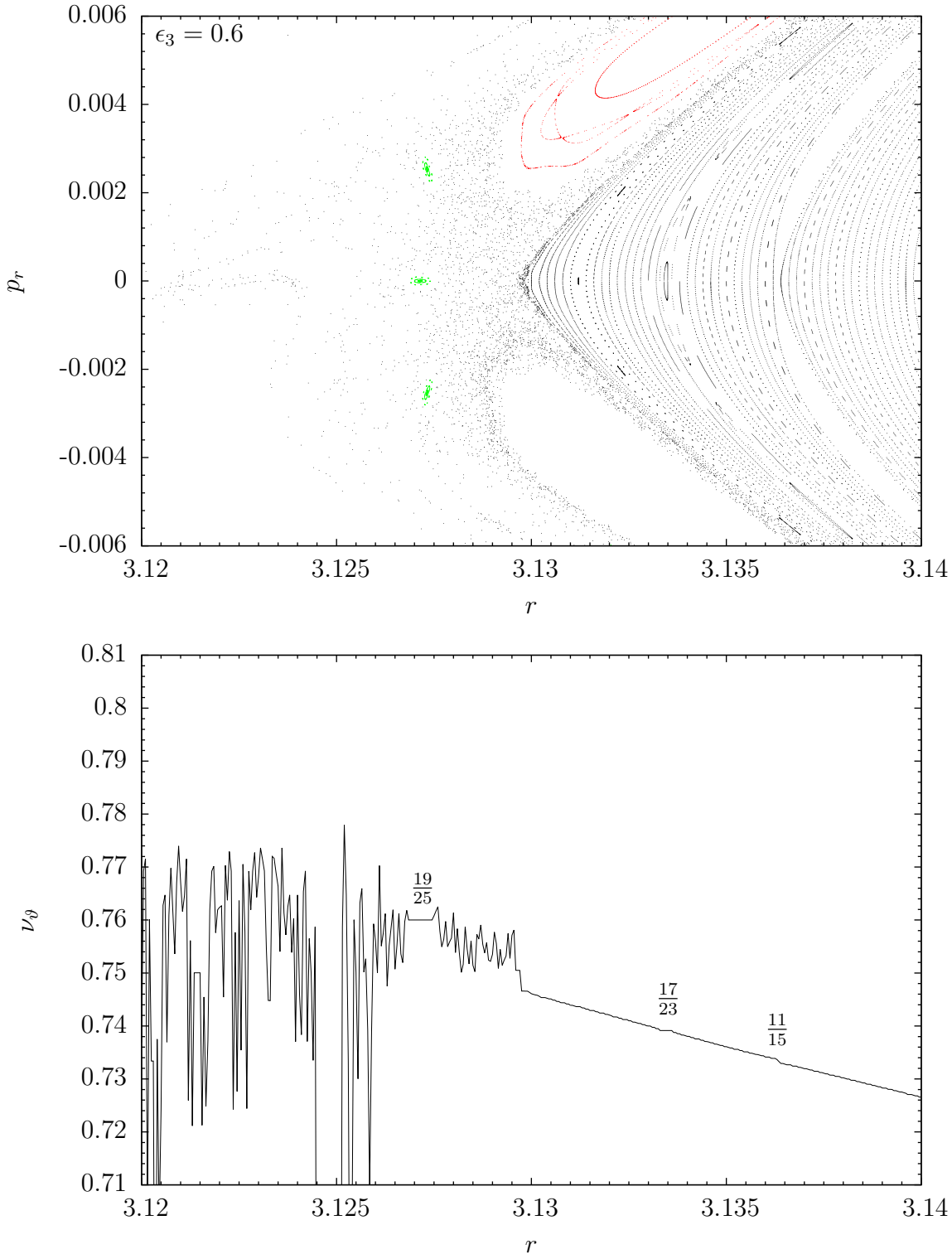

Figure 2.9: Left tip of the surface of section for $\epsilon_3 = 0.6$ with the corresponding rotation curve and fractions denoting resonances; parameters taken: $a = 0.5$, $E = 0.95$, $L_z = 2.85$.

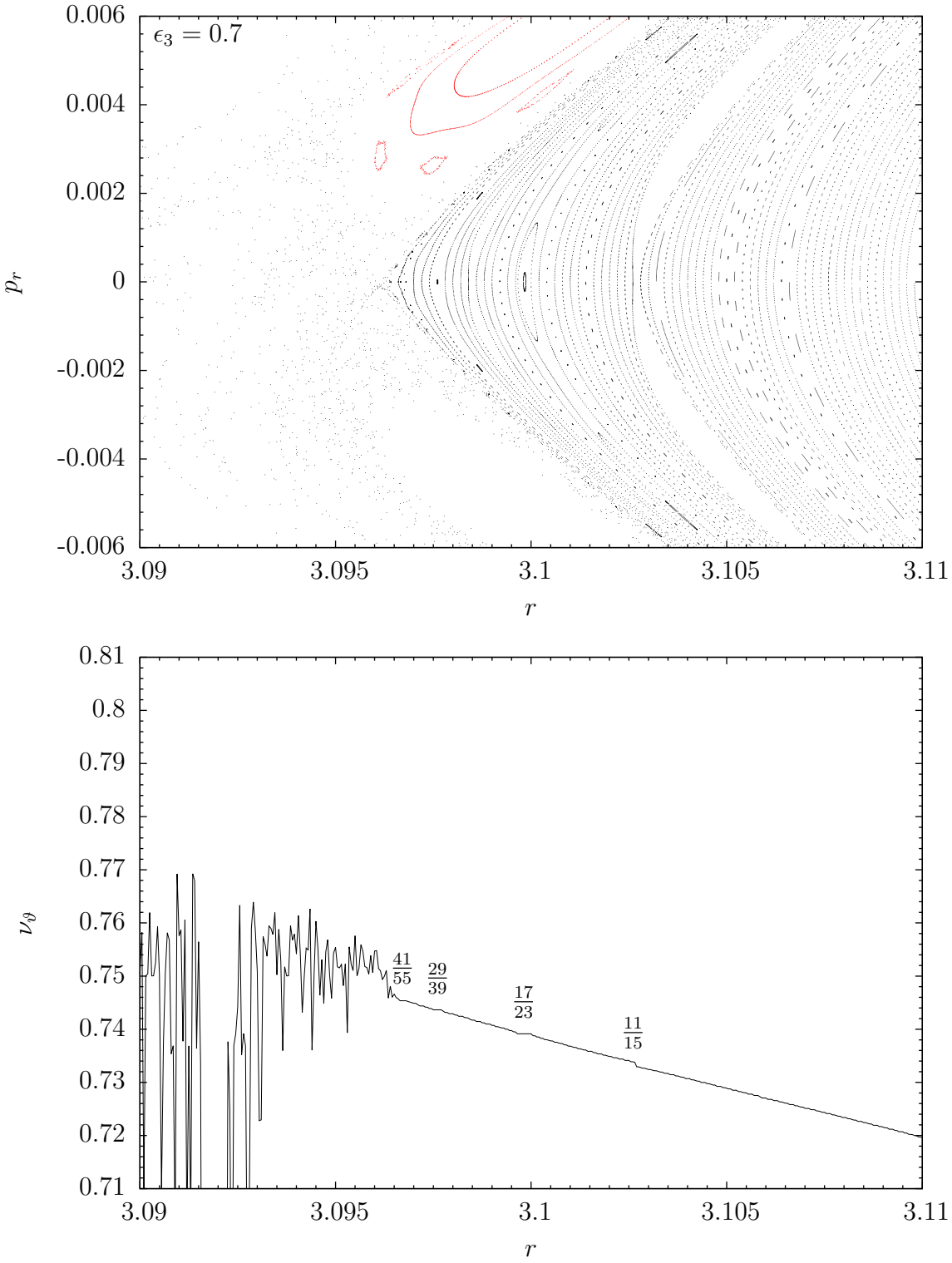

Figure 2.10: Left tip of the surface of section for $\epsilon_3 = 0.7$ with the corresponding rotation curve and fractions denoting resonances; parameters taken: $a = 0.5$, $E = 0.95$, $L_z = 2.85$.

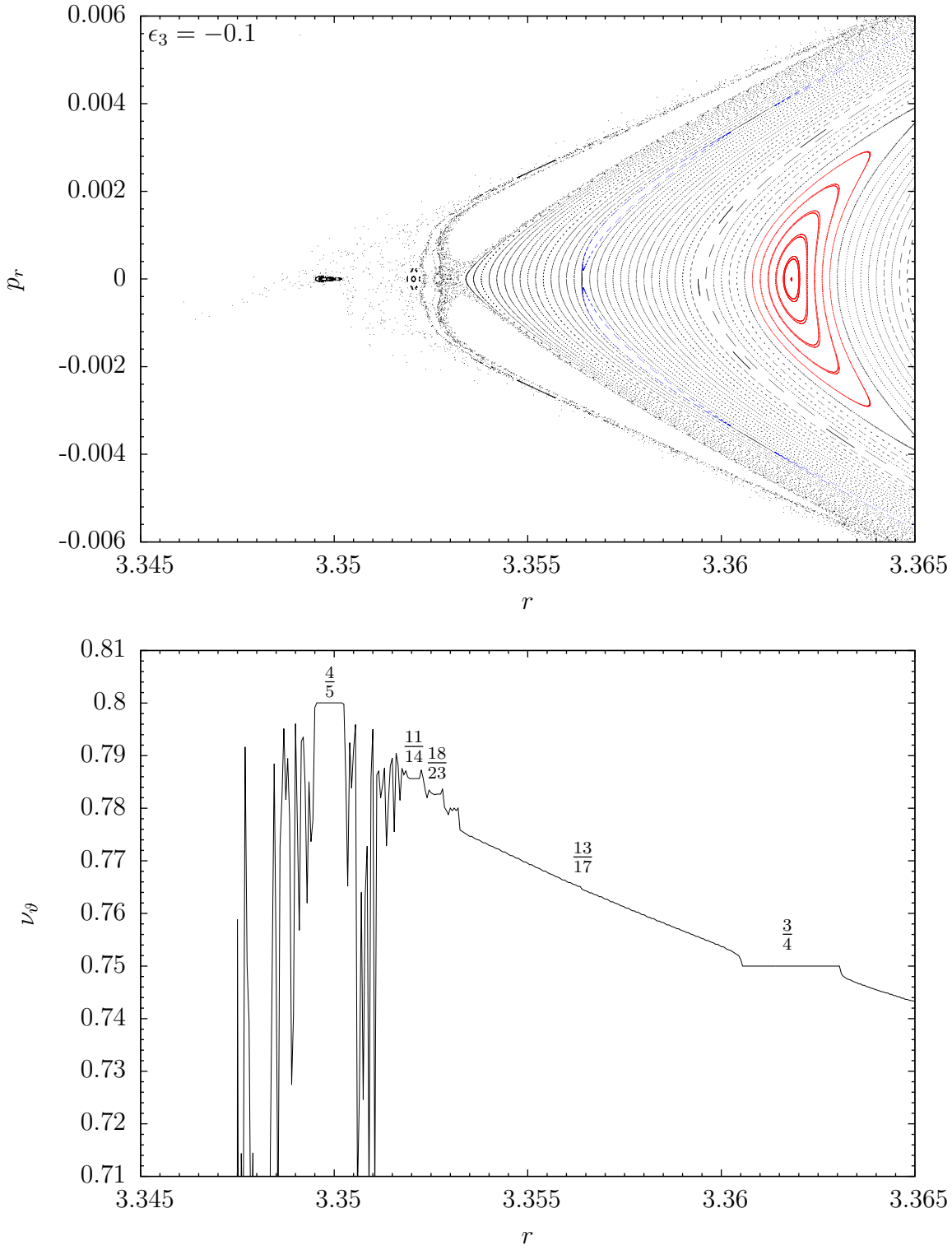

Figure 2.11: Left tip of the surface of section for $\epsilon_3 = -0.1$ with the corresponding rotation curve and fractions denoting resonances; parameters taken: $a = 0.5$, $E = 0.95$, $L_z = 2.85$.

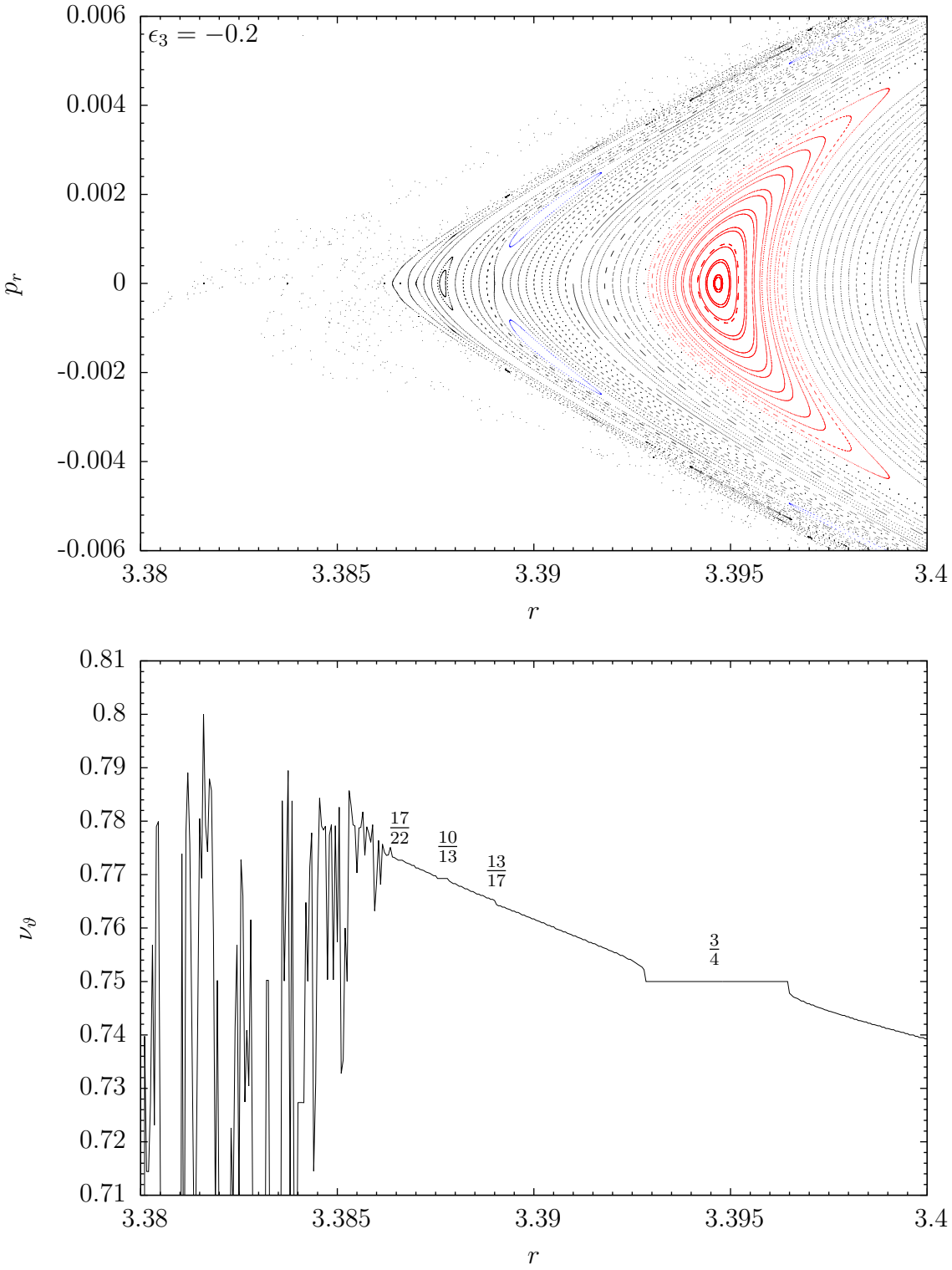

Figure 2.12: Left tip of the surface of section for $\epsilon_3 = -0.2$ with the corresponding rotation curve and fractions denoting resonances; parameters taken: $a = 0.5$, $E = 0.95$, $L_z = 2.85$.

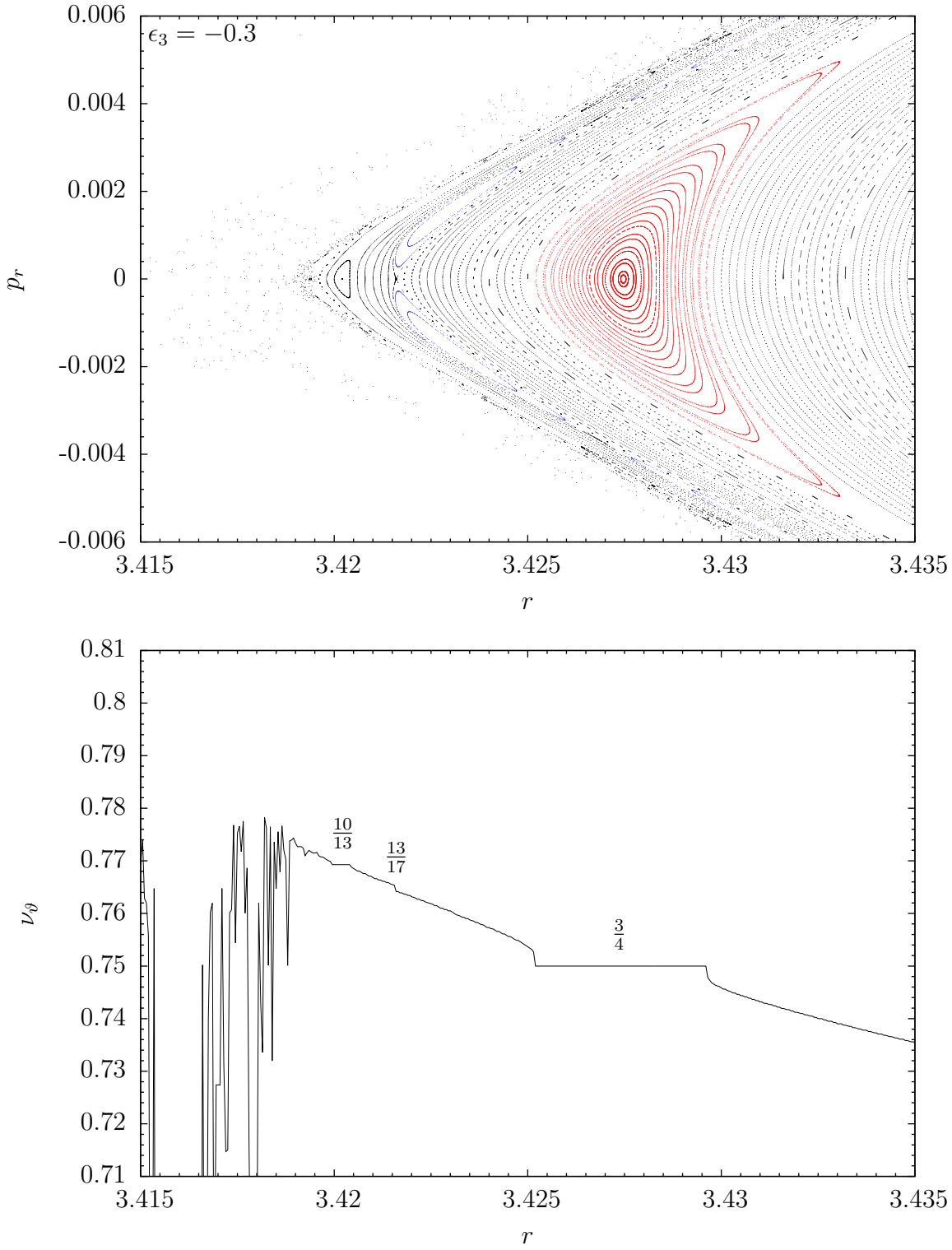

Figure 2.13: Left tip of the surface of section for $\epsilon_3 = -0.3$ with the corresponding rotation curve and fractions denoting resonances; parameters taken: $a = 0.5$, $E = 0.95$, $L_z = 2.85$.

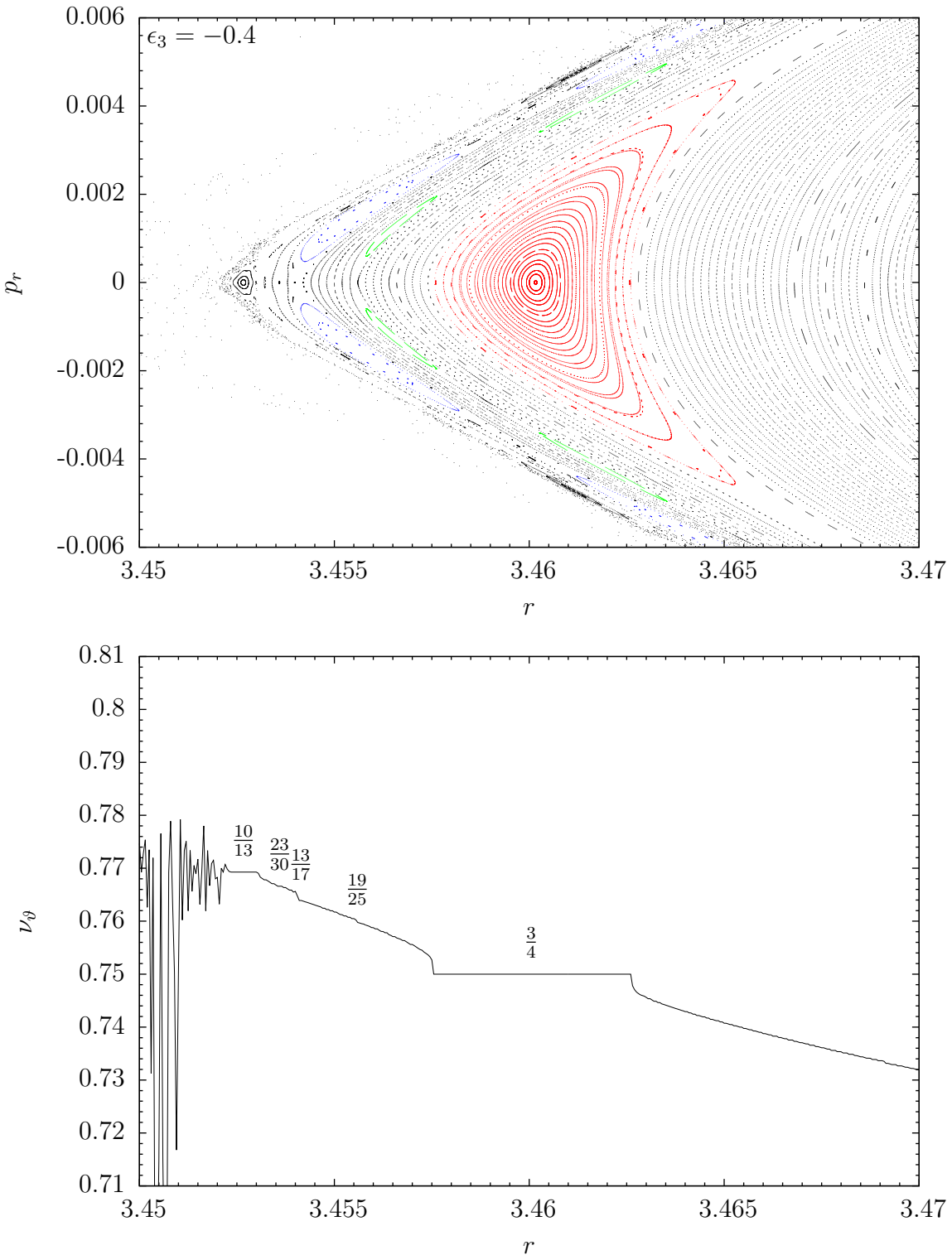

Figure 2.14: Left tip of the surface of section for $\epsilon_3 = -0.4$ with the corresponding rotation curve and fractions denoting resonances; parameters taken: $a = 0.5$, $E = 0.95$, $L_z = 2.85$.

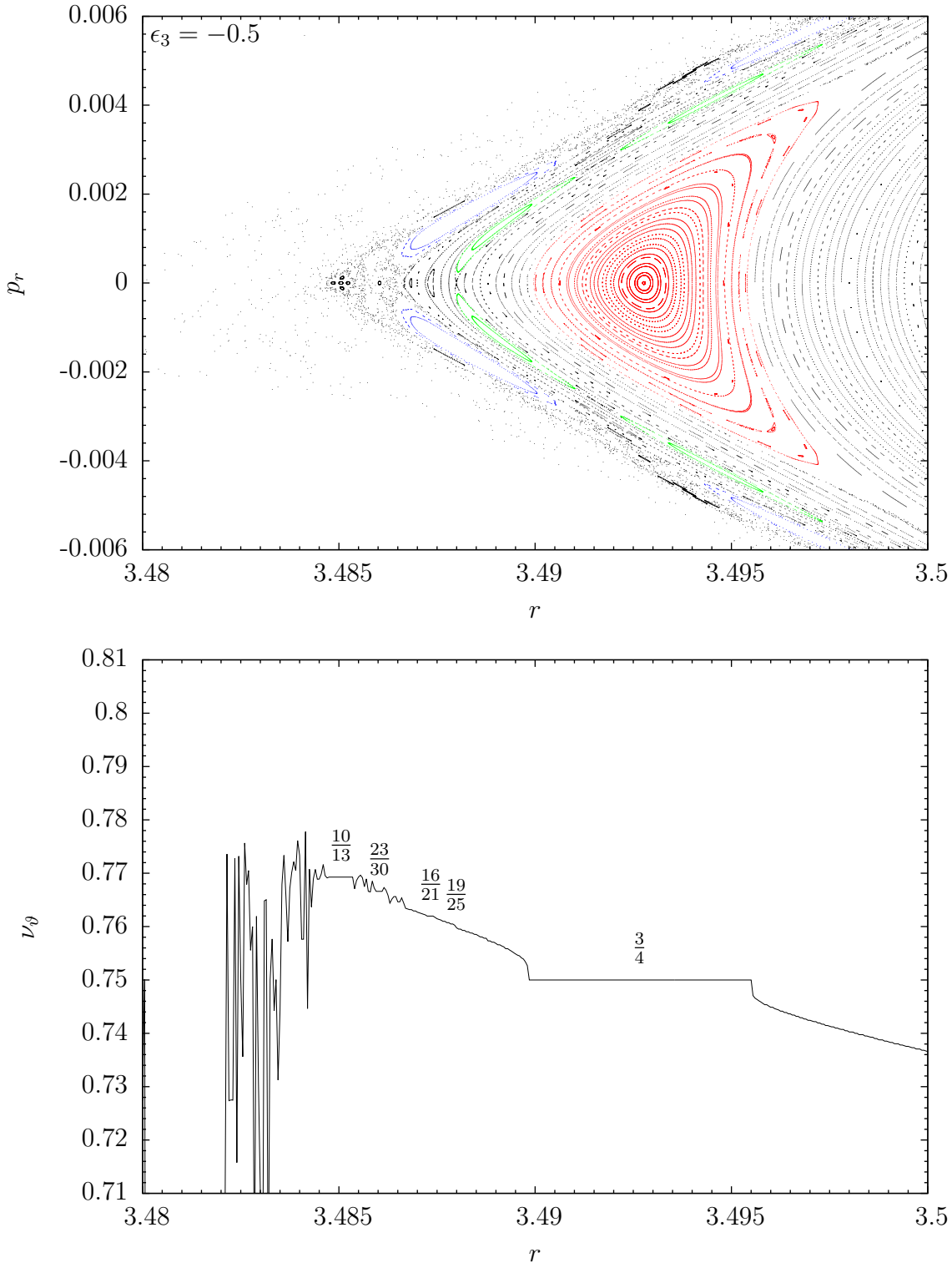

Figure 2.15: Left tip of the surface of section for $\epsilon_3 = -0.5$ with the corresponding rotation curve and fractions denoting resonances; parameters taken: $a = 0.5$, $E = 0.95$, $L_z = 2.85$.

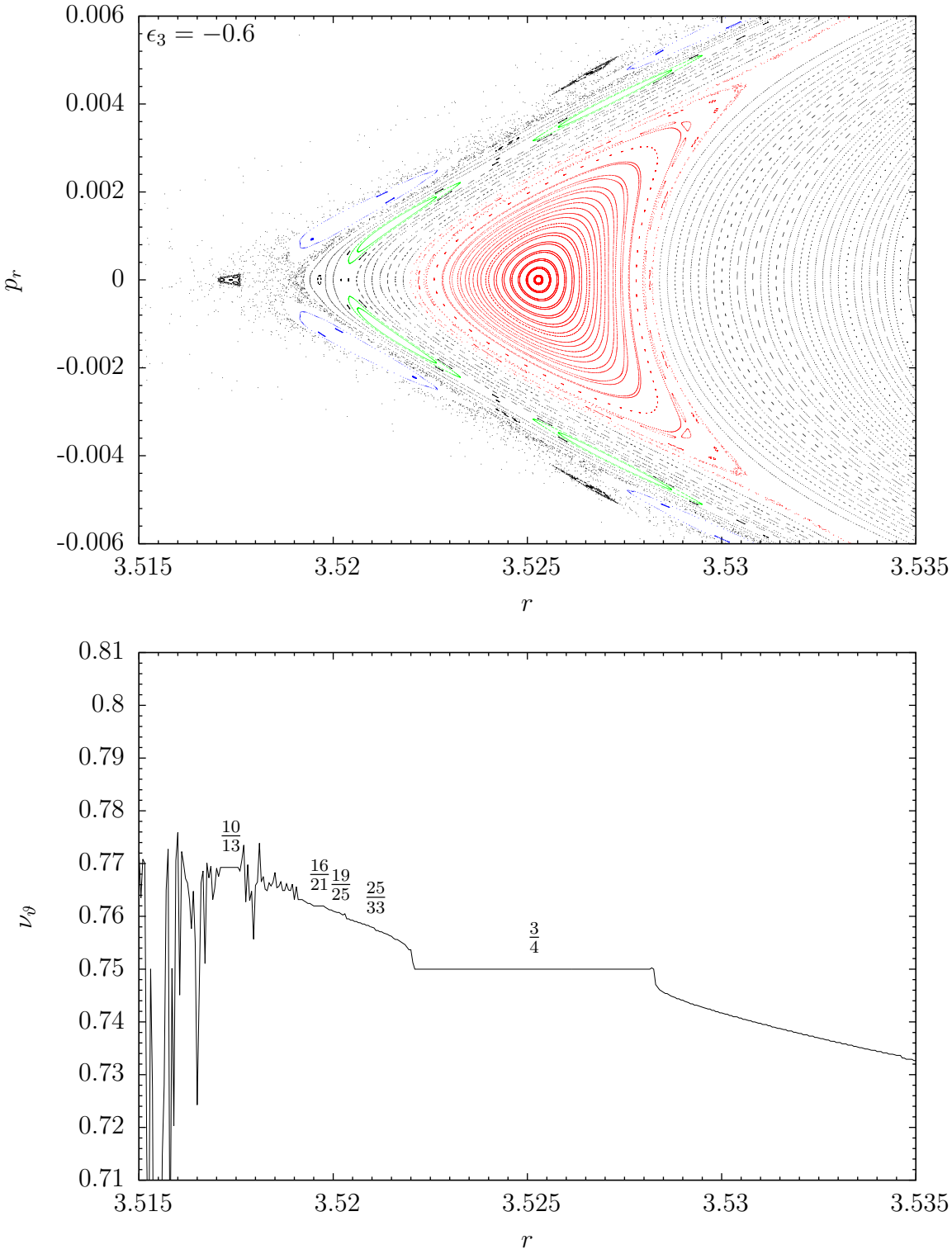

Figure 2.16: Left tip of the surface of section for $\epsilon_3 = -0.6$ with the corresponding rotation curve and fractions denoting resonances; parameters taken: $a = 0.5$, $E = 0.95$, $L_z = 2.85$.

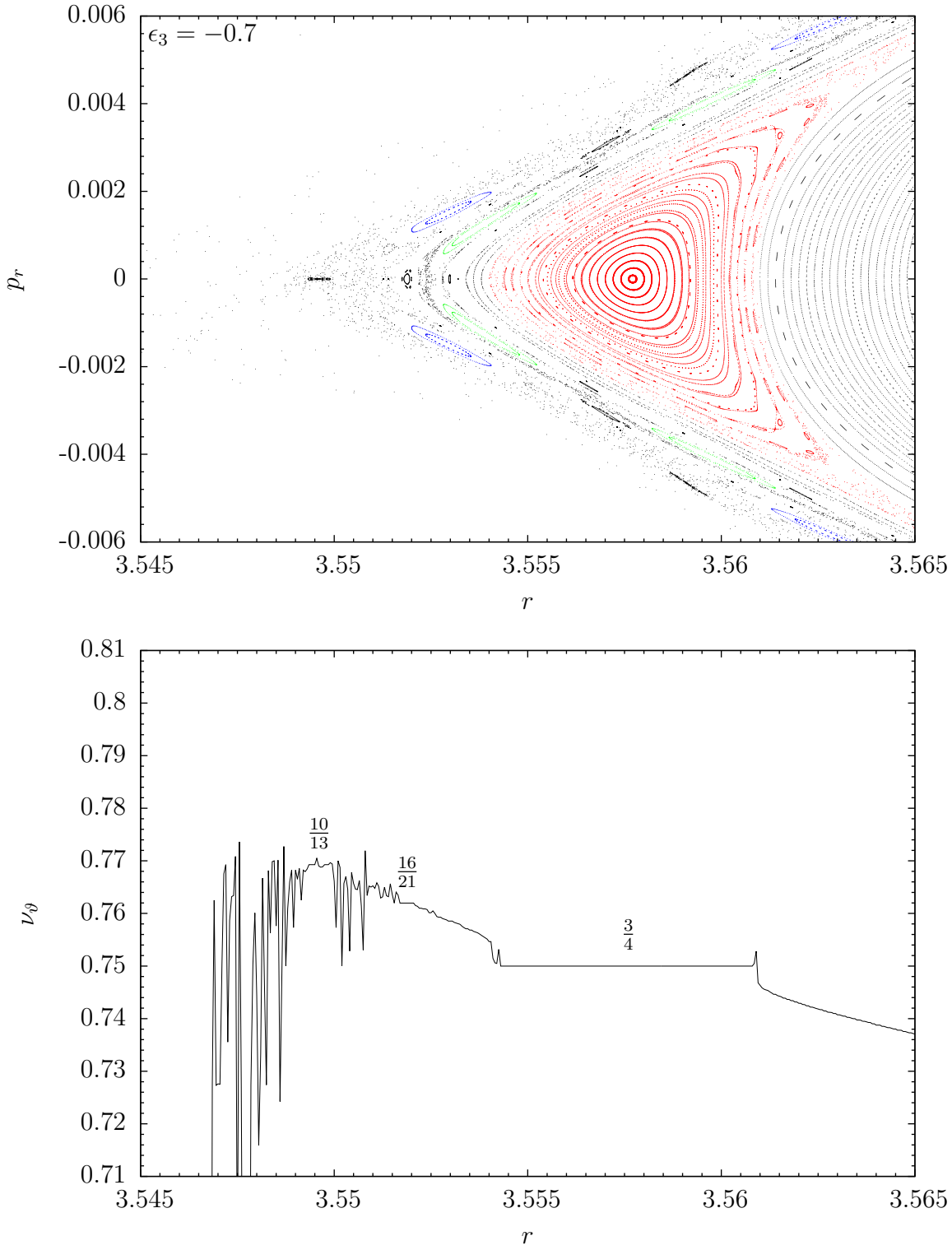

Figure 2.17: Left tip of the surface of section for $\epsilon_3 = -0.7$ with the corresponding rotation curve and fractions denoting resonances; parameters taken: $a = 0.5$, $E = 0.95$, $L_z = 2.85$.

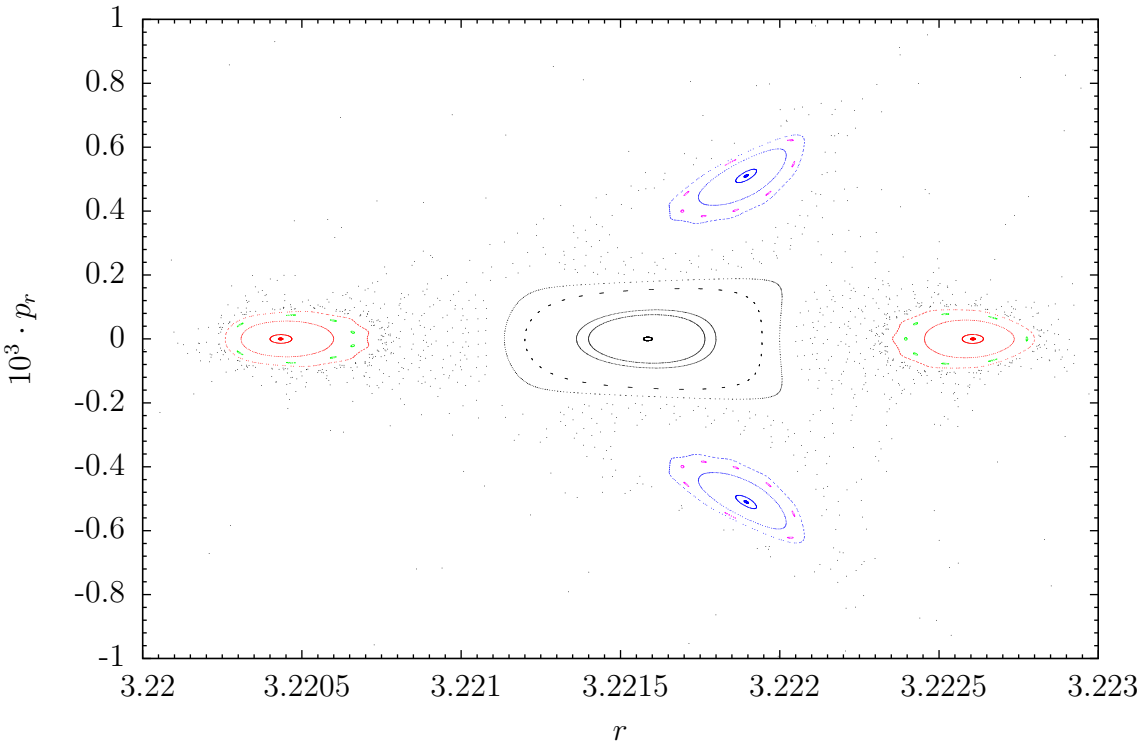

Figure 2.18: A detail of the surface of section for $\epsilon_3 = 0.3$ showing primary resonance $\frac{7}{9}$ (black), 2 secondary resonances $\frac{1}{2}$ (red and blue) and 2 tertiary resonances $\frac{7}{8}$ (green and purple); parameters taken: $a = 0.5$, $E = 0.95$, $L_z = 2.85$.

its fixed point lying on the $p_r = 0$ line near the left tip of the main island of stability is hyperbolic for both negative and positive values of ϵ_3.

Another aspect to note is that for the 3/4 resonance we see for positive values of ϵ_3 that by taking initial conditions in the leftmost island with $p_r > 0$ we didn't get any points in the symmetrical area $p_r < 0$ where there is obviously another island of the same resonance. This shows that k used in the Poincaré-Birkhoff theorem Thm. 3 truly doesn't always take on the value 1, as in this case it is at least $k = 2$. We also plot a detail of the 7/9 resonance in the $\epsilon_3 = 0.3$ case in Fig. 2.18, where we can see not only the primary resonance 7/9, but also 2 secondary resonances 1/2 (another case of $k = 2$ in Thm. 3) and even tertiary resonances 7/8, showing the self-similar structure of the phase space.

As the perturbation increases, we can see how the destruction of outer invariant circles causes resonances which were previously inside the main island of stability to move outwards into the chaotic sea; this can be best seen by watching the color-plotted resonances 3/4 and 19/25, which were surrounded by invariant circles for $\epsilon_3 = 0.4$ in Fig. 2.7, but are no longer within the main island of stability for $\epsilon_3 = 0.5$ in Fig. 2.8.

We also see that even around invariant circles, the rotation curve has a stair-like structure. This is explained in the section about dynamical spectra.

2.3 Dynamical spectra

Spectra of rotation angles have also been plotted in Figs. 2.19-2.22 for several initial conditions, iterating the orbit $N = 20000$ times and constructing the spectrum as a histogram in 750 equally long intervals in $[0 : 2\pi)$. We see in Fig. 2.19 that for an invariant circle near the center (r_c) of the main island of stability (initial condition $r_i = 9$, $r_c = 9.07878724$) the spectrum is fairly simple with two large peaks, first at a value slightly larger than 0, second at a value slightly lower than π. But as we move away from the center, we see in Fig. 2.19 for initial $r_i = 8$ that a new peak appears near the first one before again vanishing. As we approach the left tip of the main island of stability, the angles near 2π become significant (Figs. 2.20-2.22). All of these spectra were constructed for $a = 0.5$, $\epsilon_3 = 0.3$, $E = 0.95$, $L_z = 2.85$.

We see in Figs. 2.19-2.21 that, as shown in [12], the spectra are continuous for KAM curves. Also, we notice in Figs. 2.21, 2.22 that discontinuities appear for resonances and chaotic orbits.

Seeing that for all the plotted spectra the rotation angles are mostly distributed near the angles 0, π and 2π, this means that if we take two nearby initial conditions and evaluate Eq. (1.59) with the same number of iterations, the sum in the equation will differ by approximately a multiple of π, meaning that we can expect the inaccuracy of the rotation number calculation to be approximately a multiple of $1/2N$. If we take two values of ν_ϑ for two successive initial conditions on one of the rotation curves, it appears that usually they indeed follow such a law, the difference being typically close to zero or to $1/N$ [19].

2.4 Lyapunov exponents

In this section we demonstrate the calculation of the mLCE. Again, the calculations were done for $a = 0.5$, $E = 0.95$, $L_z = 2.85$. The convergence of the Lyapunov characteristic exponents is shown in Fig. 2.23 for 3 cases: a regular orbit, 2 chaotic orbits near the 3/4 resonance for different degrees of perturbation, and a strongly chaotic orbit whose mLCE converges before diffusing into the chaotic sea, which is when the FmLCE (τ) again increases, as the trajectories in the chaotic sea typically have larger LCEs. This is the phenomenon of "stickiness" [20], where trajectories outside the island of stability but close to the last KAM curve remain close to the island for very long times before diffusing into the chaotic sea. We notice that in 2.23 the orbits were evaluated for different times: the time is limited by computational abilities, in the case (b) a long time was needed for FmLCE to converge, while in the case (d) the evaluation had to be stopped because the trajectory plunged.

Eventually, we take a specific resonance and watch how the mLCE of the nearby chaotic trajectories changes when we increase the degree of perturbation. We choose the resonance 3/4, as it isn't difficult to locate a hyperbolic fixed point (it lies on the $p_r = 0$ line and the resonance is significant enough to make the chaotic zone large as well). The mLCE has been calculated for values $\epsilon_3 = 0.1, 0.2, 0.3, 0.4, 0.5$ with $a = 0.5$, $E = 0.95$ and $L_z = 2.85$ (the cases $\epsilon_3 = 0.1, 0.3, 0.5$ were used in Fig. 2.23). The computed mLCEs are plotted in Fig. 2.24. As we see in 2.23, the FmLCE still oscillates even after the Lyapunov time,

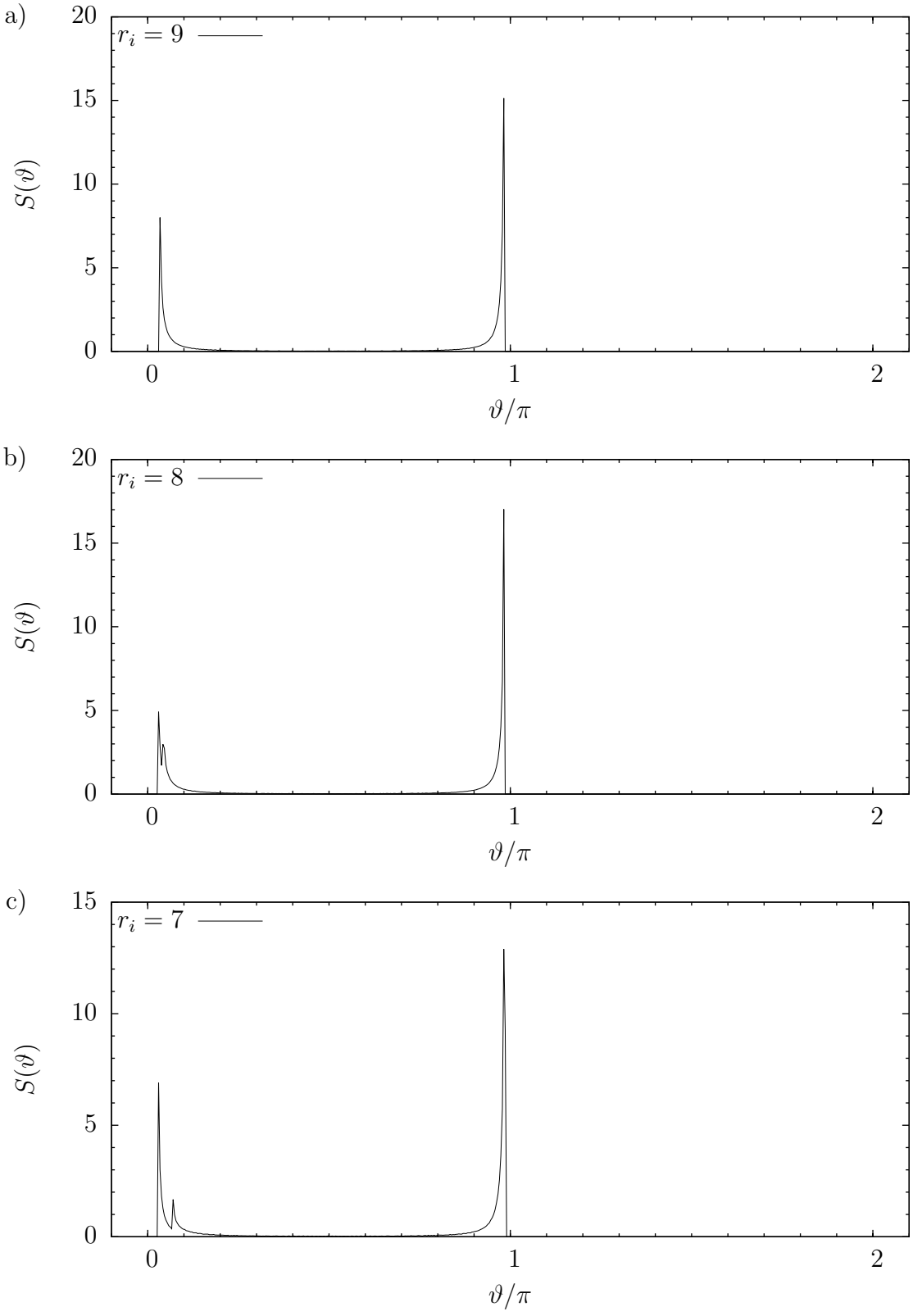

Figure 2.19: Dynamical spectra of regular orbits with initial a) $r_i = 9$, b) $r_i = 8$, c) $r_i = 7$

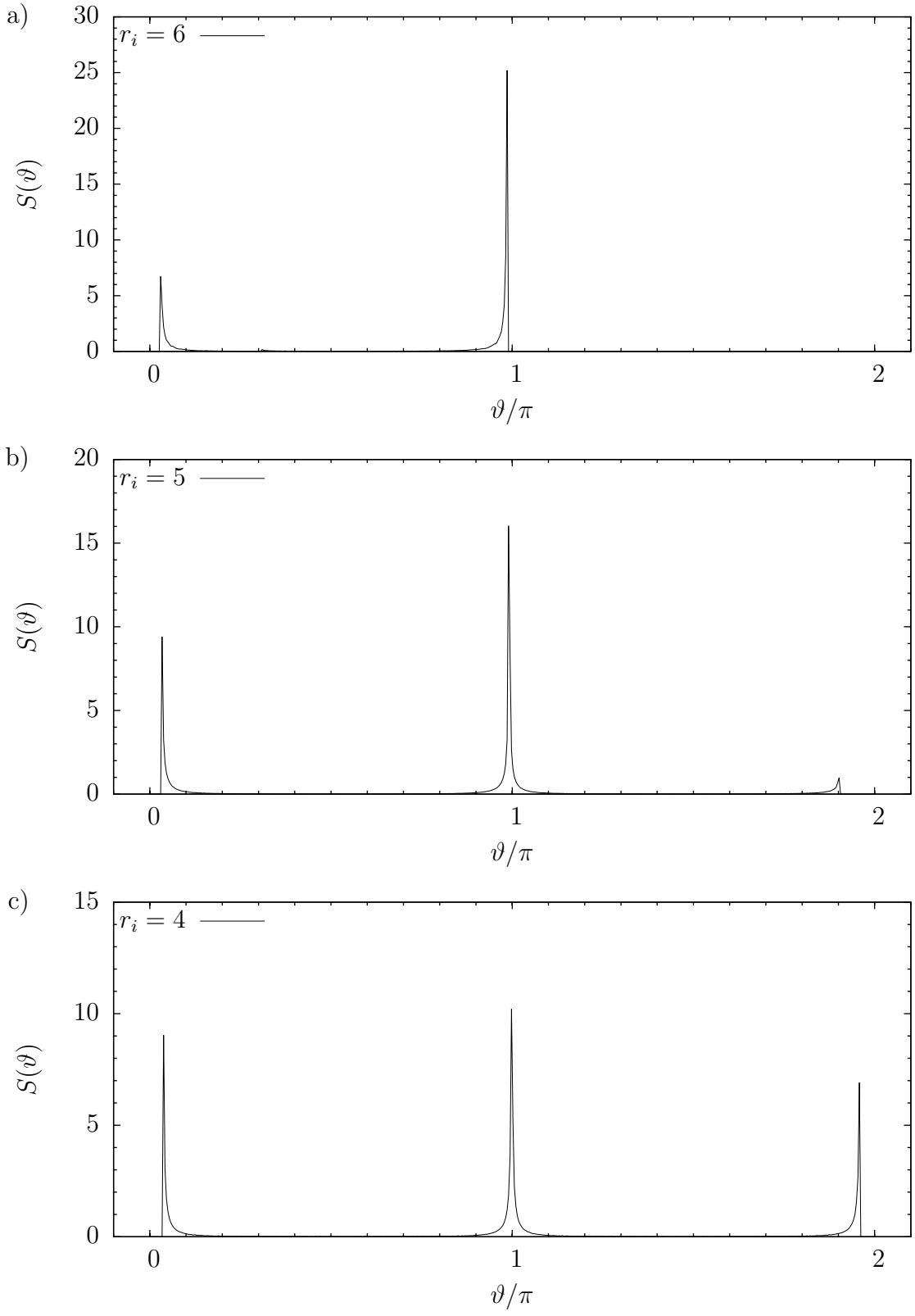

Figure 2.20: Dynamical spectra of regular orbits with initial a) $r_i = 6$, b) $r_i = 5$, c) $r_i = 4$

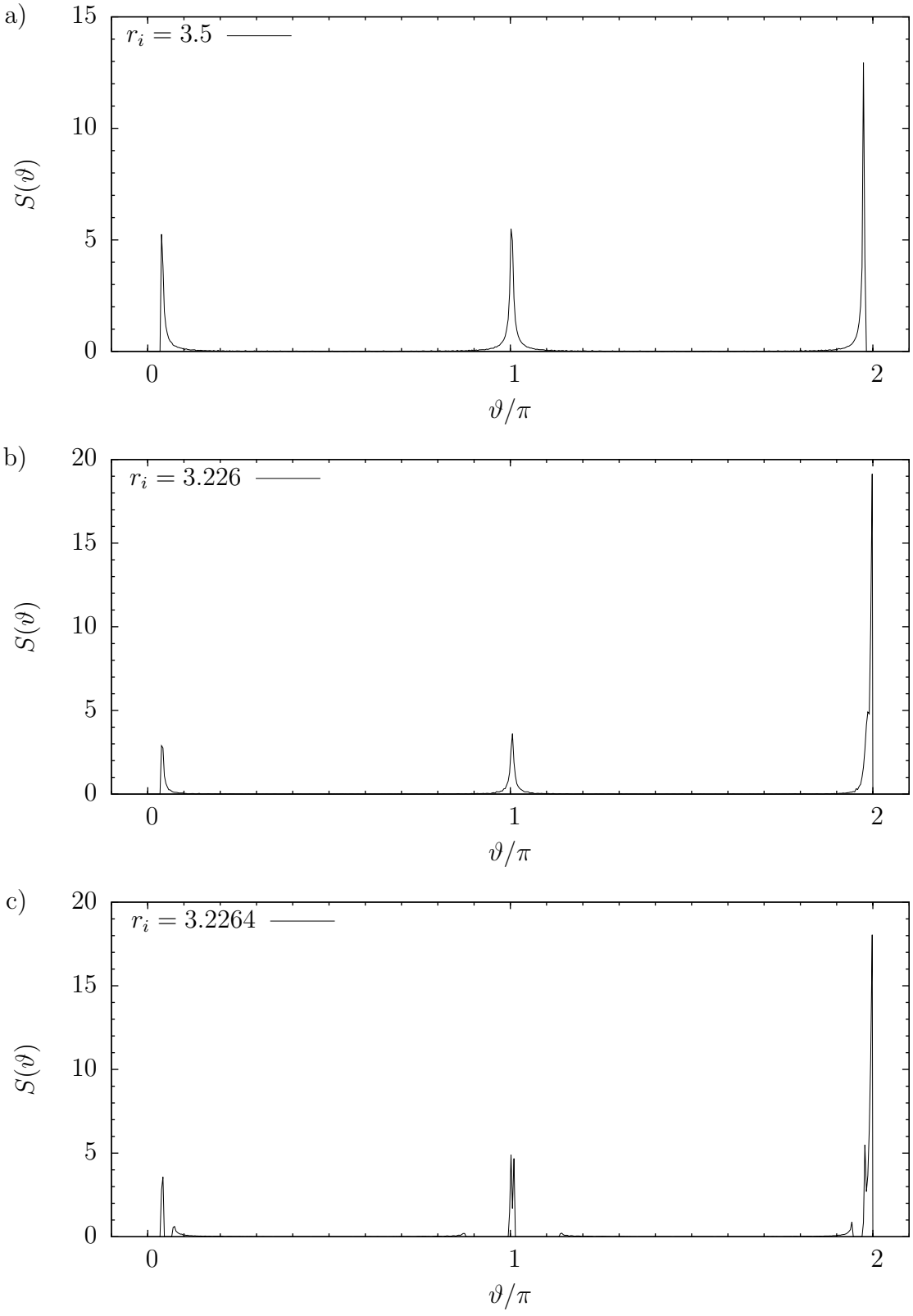

Figure 2.21: Dynamical spectra of regular orbits with initial a) $r_i = 3.5$ (KAM curve), b) $r_i = 3.226$ (KAM curve), c) $r_i = 3.2264$ (19/25 resonance)

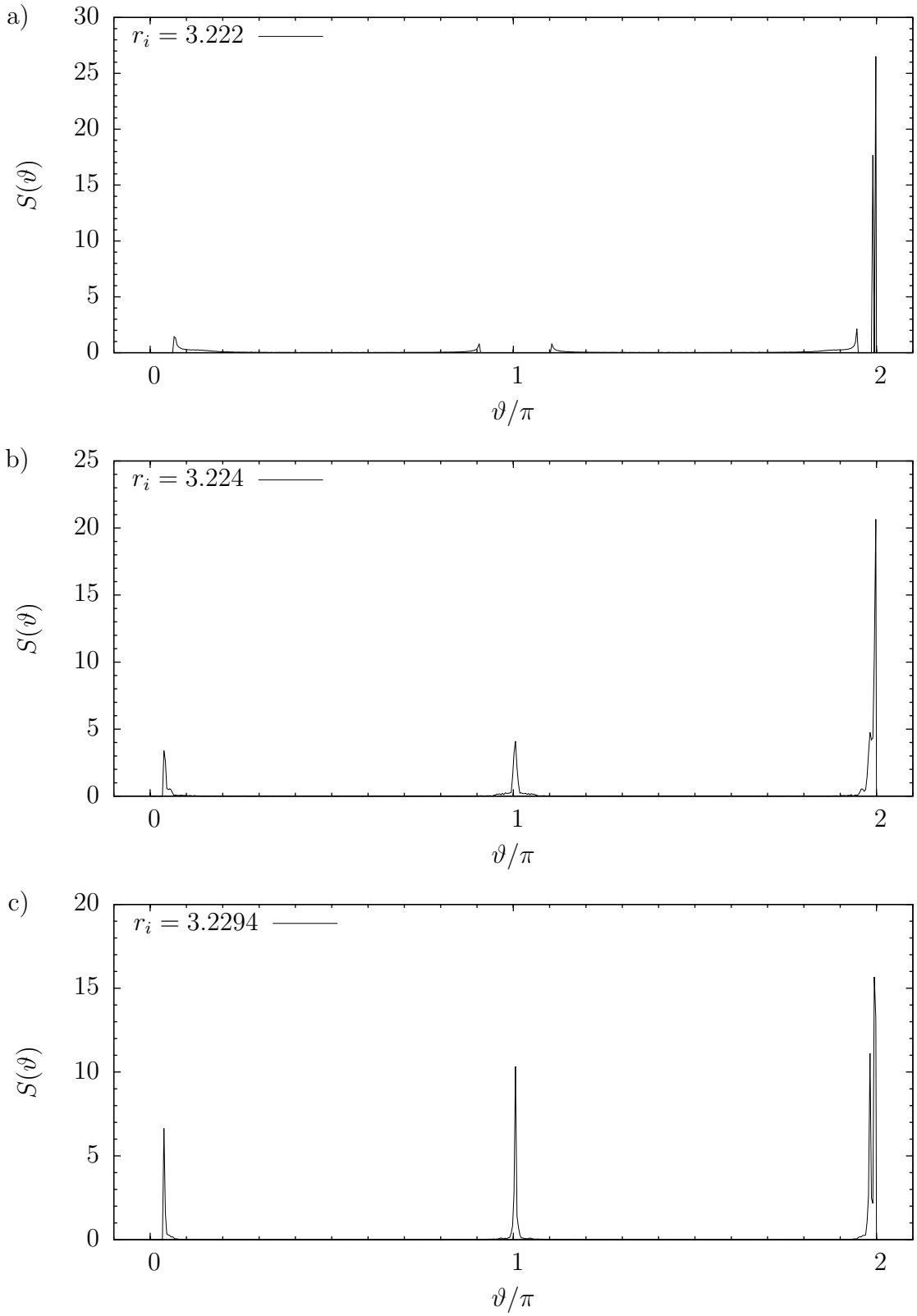

Figure 2.22: Dynamical spectra of orbits with initial a) $r_i = 3.222$ (regular, 7/9 resonance), b) $r_i = 3.224$ (in the chaotic sea, plunged after 7354 iterations), c) $r_i = 3.2294$ (in an inside chaotic zone, near the 3/4 resonance)

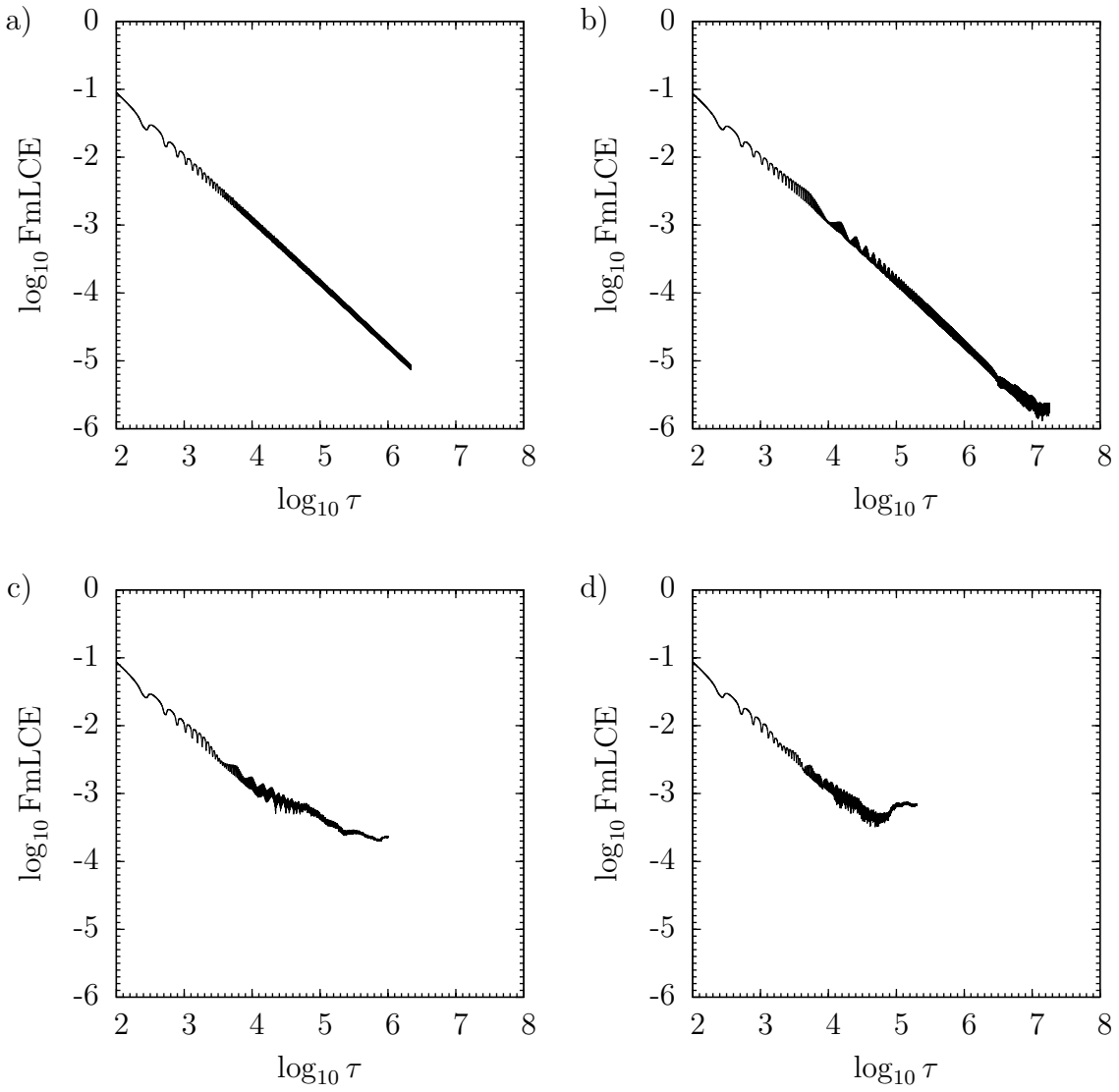

Figure 2.23: Convergence of the Lyapunov exponents for a) a regular trajectory ($\epsilon_3 = 0.3$, $r_i = 3.226$), and for 3 chaotic trajectories b) ($\epsilon_3 = 0.1$, $r_i = 3.29581$), c) ($\epsilon_3 = 0.3$, $r_i = 3.2294$), d) ($\epsilon_3 = 0.5$, $r_i = 3.1626$)

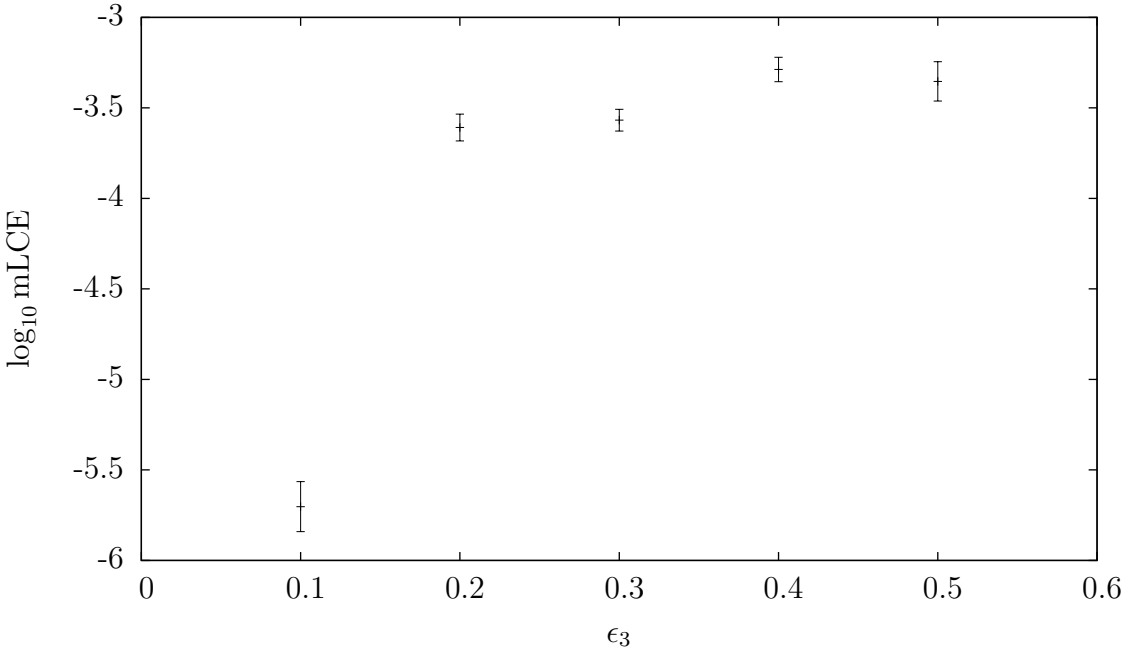

Figure 2.24: Lyapunov exponents of chaotic trajectories near the 3/4 resonance as a function of ϵ_3

the error bars account for this oscillation. We see in Fig. 2.24 that the mLCE is orders of magnitude lower for $\epsilon_3 = 0.1$ than for higher values, for which it doesn't appear to grow significantly anymore. This could be caused by merging of two nearby resonances.

Conclusion

We have summarized the basics of theory of dynamical systems, introduced the notion of integrability, chaos, symplectic mappings and described their properties. A program has been written in C to evolve geodesic trajectories in the Johannsen-Psaltis spacetime, to plot surfaces of section, to evolve geodesic deviation equations and to calculate Lyapunov exponents. Then we have employed numerical examples by using the above program to show that chaos emerges in this spacetime when deviating from the Kerr metric by a perturbation parameter. Thus, we have proven that geodesic motion in the Johannsen-Psaltis metric corresponds to a non-integrable system.

The point of this research is to understand the motion of massive test particles in a non-integrable spacetime background. Even though a test particle should be added to the energy-stress tensor and therefore alter the geometry of the spacetime, geodesic motion is a good approximation of the motion of a compact object which is much less massive than the central compact object. The results of such research might have implications in the emission of gravitational wave signals from extreme mass ratio inspirals, i.e. a stellar mass black hole or a neutron star inspiraling into a supermassive black hole of mass on the order of $10^5 - 10^7$ solar masses. If we were to observe the gravitational wave signature of such an event, we might be able to decode if this signal comes from an orbit with chaotic behavior, which would indicate the presence of a non-integrable spacetime background, possibly of a non-Kerr spacetime. Other possible sources of non-integrability include other matter nearby, e.g. an accretion disk.

Such observation is currently not in our capabilities (so far we have only measured a few events of gravitational waves, where the progenitor consists of two black holes with comparable mass); it is, however, possible that in the next decade the European New Gravitational Wave Observatory (NGO) [18] will be launched. It will be able to detect EMRIs into supermassive compact objects at the centers of galaxies. This will allow us to conduct strong-field experiments and make conclusions on the Kerr hypothesis [3] and, possibly, on the no-hair theorem [2].

Bibliography

[1] Tim Johannsen and Dimitrios Psaltis. Metric for rapidly spinning black holes suitable for strong-field tests of the no-hair theorem. *Phys. Rev. D*, 83:124015, Jun 2011.

[2] B. Carter. Axisymmetric black hole has only two degrees of freedom. *Phys. Rev. Lett.*, 26:331–333, Feb 1971.

[3] Joao Miguel Arsenio Rico. The Kerr black hole hypothesis: a review of methods and results. Master's thesis, Lisbon, CENTRA, 2013.

[4] Brandon Carter. Global structure of the kerr family of gravitational fields. *Phys. Rev.*, 174:1559–1571, Oct 1968.

[5] Wolfgang Rindler. *Relativity: special, general, and cosmological*. Oxford Univ. Press, 2 edition, 2006.

[6] L.D Landau and E.M Lifshitz. *Course of theoretical physics. Mechanics*. Pergamon Press, 1959.

[7] A.J. Lichtenberg and M.A. Lieberman. *Regular and Chaotic Dynamics*. Second Edition. Springer-Verlag, New York, 1992.

[8] V.I Arnold. *Mathematical methods of classical mechanics*. Springer, 1989.

[9] Georgios Lukes-Gerakopoulos, Matthaios Katsanikas, Panos A. Patsis, and Jonathan Seyrich. Dynamics of a spinning particle in a linear in spin hamiltonian approximation. *Phys. Rev. D*, 94:024024, Jul 2016.

[10] J. D. Meiss. Symplectic maps, variational principles, and transport. *Rev. Mod. Phys.*, 64:795–848, Jul 1992.

[11] Jacques Laskar. Frequency analysis of a dynamical system. *Celestial Mechanics and Dynamical Astronomy*, 56(1):191–196, 1993.

[12] N. Voglis and C. Efthymiopoulos. Angular dynamical spectra. a new method for determining frequencies, weak chaos and cantori. *Journal of Physics A: Mathematical and General*, 31(12):2913, 1998.

[13] Bernd Aulbach. The fundamental existence theorem on invariant fiber bundles. *Journal of Difference Equations and Applications*, 3(5-6):267–312, 1998.

[14] Edson A. Coayla-Teran, Salah-Eldin A. Mohammed, and Paulo Régis C. Ruffino. Hartman-grobman theorems along hyperbolic stationary trajectories. *Discrete and Continuous Dynamical Systems*, 17(2):281–292, 2007.

[15] R.L. Devaney. *An Introduction to Chaotic Dynamical Systems*. Addison-Wesley advanced book program. Addison-Wesley, 1989.

[16] J. Banks, J. Brooks, G. Cairns, G. Davis, and P. Stacey. On devaney's definition of chaos. *The American Mathematical Monthly*, 99(4):332–334, 1992.

[17] Georgios Lukes-Gerakopoulos. Adjusting chaotic indicators to curved spacetimes. *Phys. Rev. D*, 89:043002, Feb 2014.

[18] Georgios Lukes-Gerakopoulos. Nonintegrability of the zipoy-voorhees metric. *Phys. Rev. D*, 86:044013, Aug 2012.

[19] N. Voglis, G. Contopoulos, and C. Efthymiopoulos. Detection of ordered and chaotic motion using the dynamical spectra. *Celestial Mechanics and Dynamical Astronomy*, 73(1):211–220, 1999.

[20] R. Dvorak, G. Contopoulos, Ch. Efthymiopoulos, and N. Voglis. "stickiness" in mappings and dynamical systems. *Planetary and Space Science*, 46(11):1567 – 1578, 1998.

List of Figures

Appendices

A. Properties of the Johannsen-Psaltis spacetime

While the calculation of the inverse metric tensor may get tedious in a general four-dimensional spacetime, the symmetries of this metric simplify the task greatly. As the only non-diagonal elements of the metric tensor are the ones corresponding to the coordinates t and ϕ, giving the metric block diagonal form with three blocks of dimensions 1, 1 and 2. This simplifys the calculation of the contravariant metric

$$g^{tt} = \frac{g_{\phi\phi}}{g_{tt}g_{\phi\phi} - g_{t\phi}^2}, \tag{A.1a}$$

$$g^{\phi\phi} = \frac{g_{tt}}{g_{tt}g_{\phi\phi} - g_{t\phi}^2}, \tag{A.1b}$$

$$g^{t\phi} = g^{\phi t} = -\frac{g_{t\phi}}{g_{tt}g_{\phi\phi} - g_{t\phi}^2}, \tag{A.1c}$$

$$g^{\theta\theta} = \frac{1}{g_{\theta\theta}}, \tag{A.1d}$$

$$g^{rr} = \frac{1}{g_{rr}}. \tag{A.1e}$$

In the text we work with the integrals of motion (1.29). Using the contravariant metric components (A.1) we can express

$$u^t = -\frac{g_{\phi\phi}E + g_{t\phi}L_z}{g_{tt}g_{\phi\phi} - g_{t\phi}^2}, \tag{A.2a}$$

$$u^\phi = \frac{g_{t\phi}E + g_{tt}L_z}{g_{tt}g_{\phi\phi} - g_{t\phi}^2}, \tag{A.2b}$$

which is useful for numerical calculations.

To solve all the equations involved in this thesis we need the Christoffel symbols of the second kind and their derivatives, their calculation includes the calculation of the first and second derivatives of the metric.

$$\Sigma_{,r} = 2r, \quad \Sigma_{,\theta} = -2a^2 \sin\theta\cos\theta \tag{A.3a}$$

$$h_{,r} = h\left(\frac{1}{r} - \frac{2\Sigma_{,r}}{\Sigma}\right), \quad h_{,\theta} = -2\frac{\Sigma_{,\theta}}{\Sigma}\cdot h \tag{A.3b}$$

$$\Delta_{,r} = 2\left(r - M\right), \quad \Delta_{,\theta} = 0 \tag{A.3c}$$

$$\left(\omega^2\right)_{,r} = 2r, \quad \left(\omega^2\right)_{,\theta} = 0 \tag{A.3d}$$

$$\Lambda_{,r} = 2\omega^2\left(\omega^2\right)_{,r} - a^2\Delta_{,r}\sin^2\theta \tag{A.3e}$$

$$\Lambda_{,\theta} = -2a^2\Delta\sin\theta\cos\theta \tag{A.3f}$$

$$B_{,r} = \Delta_{,r} + a^2 h_{,r} \sin^2\theta \tag{A.4a}$$
$$B_{,\theta} = a^2 h_{,\theta} \sin^2\theta + 2a^2 h \sin\theta\cos\theta \tag{A.4b}$$
$$C_{,r} = C\left(\frac{\Lambda_{,r}}{\Lambda} - \frac{\Sigma_{,r}}{\Sigma}\right) \tag{A.4c}$$
$$C_{,\theta} = C\left(\frac{\Lambda_{,\theta}}{\Lambda} - \frac{\Sigma_{,\theta}}{\Sigma} + 2\frac{\cos\theta}{\sin\theta}\right) \tag{A.4d}$$
$$F_{,r} = -\frac{2Mr}{\Sigma^2}\Sigma_{,r} + \frac{2M}{\Sigma} \tag{A.4e}$$
$$F_{,\theta} = -\frac{2Mr}{\Sigma^2}\Sigma_{,\theta} \tag{A.4f}$$
$$D_{,r} = D\left(\frac{h_{,r}}{h} + \frac{F_{,r}}{F}\right) \tag{A.4g}$$
$$D_{,\theta} = D\left(\frac{h_{,\theta}}{h} + \frac{F_{,\theta}}{F} + 4\frac{\cos\theta}{\sin\theta}\right) \tag{A.4h}$$

$$\Sigma_{,rr} = 2, \quad \Sigma_{,\theta r} = \Sigma_{,r\theta} = 0, \quad \Sigma_{,\theta\theta} = 2a^2\left(1 - 2\cos^2\theta\right) \tag{A.5a}$$
$$h_{,rr} = \frac{h_{,r}^2}{h} + h\left(2\frac{\Sigma_{,r}^2}{\Sigma^2} - 2\frac{\Sigma_{,rr}}{\Sigma} - \frac{1}{r^2}\right) \tag{A.5b}$$
$$h_{,\theta r} = h_{,r\theta} = \frac{h_{,\theta}h_{,r}}{h} + 2\frac{h\Sigma_{,\theta}\Sigma_{,r}}{\Sigma^2} \tag{A.5c}$$
$$h_{,\theta\theta} = \frac{h_{,\theta}^2}{h} + 2h\frac{\Sigma_{,\theta}^2}{\Sigma^2} - 2h\frac{\Sigma_{,\theta\theta}}{\Sigma} \tag{A.5d}$$
$$\Delta_{,rr} = 2, \quad \Delta_{,\theta r} = \Delta_{,r\theta} = \Delta_{,\theta\theta} = 0 \tag{A.5e}$$
$$\left(\omega^2\right)_{,rr} = 2, \quad \left(\omega^2\right)_{,\theta r} = \left(\omega^2\right)_{,r\theta} = \left(\omega^2\right)_{,\theta\theta} = 0 \tag{A.5f}$$
$$\Lambda_{,rr} = 2\left(\omega^2\right)_{,r}^2 + 2\omega^2\left(\omega^2\right)_{,rr} - a^2\Delta_{,rr}\sin^2\theta \tag{A.5g}$$
$$\Lambda_{,\theta r} = \Lambda_{,r\theta} = -2a^2\Delta_{,r}\sin\theta\cos\theta \tag{A.5h}$$
$$\Lambda_{,\theta\theta} = 2a^2\Delta\left(1 - 2\cos^2\theta\right) \tag{A.5i}$$

$$B_{,rr} = \Delta_{,rr} + a^2 h_{,rr} \sin^2\theta \tag{A.6a}$$
$$B_{,\theta r} = B_{,r\theta} = a^2 h_{,\theta r} \sin^2\theta + 2a^2 h_{,r} \sin\theta\cos\theta \tag{A.6b}$$
$$B_{,\theta\theta} = a^2\left[4h_{,\theta}\sin\theta\cos\theta + 2h\left(1-2\sin^2\theta\right) + h_{,\theta\theta}\sin^2\theta\right] \tag{A.6c}$$
$$C_{,rr} = \frac{C_{,r}^2}{C} + C\left(\frac{\Lambda\Lambda_{,rr} - \Lambda_{,r}^2}{\Lambda^2} - \frac{\Sigma\Sigma_{,rr} - \Sigma_{,r}^2}{\Sigma^2}\right) \tag{A.6d}$$
$$C_{,\theta r} = C_{,r\theta} = \frac{C_{,\theta}C_{,r}}{C} + C\left(\frac{\Lambda_{,\theta r}\Lambda - \Lambda_{,\theta}\Lambda_{,r}}{\Lambda^2} + \frac{\Sigma_{,\theta}\Sigma_{,r}}{\Sigma^2}\right) \tag{A.6e}$$
$$C_{,\theta\theta} = \frac{C_{,\theta}^2}{C} + C\left(\frac{\Lambda\Lambda_{,\theta\theta} - \Lambda_{,\theta}^2}{\Lambda^2} - \frac{\Sigma\Sigma_{,\theta\theta} - \Sigma_{,\theta}^2}{\Sigma^2} - \frac{2}{\sin^2\theta}\right) \tag{A.6f}$$
$$F_{,rr} = \frac{4Mr}{\Sigma^3}\Sigma_{,r}^2 - \frac{2Mr}{\Sigma^2}\Sigma_{,rr} - \frac{4M}{\Sigma^2}\Sigma_{,r} \tag{A.6g}$$
$$F_{,\theta r} = F_{,r\theta} = \frac{4Mr}{\Sigma^3}\Sigma_{,r}\Sigma_{,\theta} - \frac{2M}{\Sigma^2}\Sigma_{,\theta} \tag{A.6h}$$
$$F_{,\theta\theta} = \frac{4Mr}{\Sigma^3}\Sigma_{,\theta}^2 - \frac{2Mr}{\Sigma^2}\Sigma_{,\theta\theta} \tag{A.6i}$$
$$D_{,rr} = \frac{D_{,r}^2}{D} + D\left(\frac{hh_{,rr} - h_{,r}^2}{h^2} + \frac{F_{,rr}F - F_{,r}^2}{F^2}\right) \tag{A.6j}$$
$$D_{,\theta r} = D_{,r\theta} = \frac{D_{,\theta}D_{,r}}{D} + D\left(\frac{hh_{,\theta r} - h_{,r}h_{,\theta}}{h^2} + \frac{FF_{,\theta r} - F_{,\theta}F_{,r}}{F^2}\right) \tag{A.6k}$$
$$D_{,\theta\theta} = \frac{D_{,\theta}^2}{D} + D\left(\frac{hh_{,\theta\theta} - h_{,\theta}^2}{h^2} + \frac{FF_{,\theta\theta} - F_{,\theta}^2}{F^2} - \frac{4}{\sin^2\theta}\right) \tag{A.6l}$$

$$g_{tt,r} = -h_{,r}\left(1 - \frac{2Mr}{\Sigma}\right) - (1+h)\left(\frac{2Mr}{\Sigma^2}\Sigma_{,r} - \frac{2M}{\Sigma}\right) \tag{A.7a}$$
$$g_{tt,\theta} = -h_{,\theta}\left(1 - \frac{2Mr}{\Sigma}\right) - (1+h)\frac{2Mr}{\Sigma^2}\Sigma_{,\theta} \tag{A.7b}$$
$$g_{t\phi,r} = g_{t\phi}\left(\frac{h_{,r}}{1+h} + \frac{1}{r} - \frac{\Sigma_{,r}}{\Sigma}\right) \tag{A.7c}$$
$$g_{t\phi,\theta} = g_{t\phi}\left(\frac{h_{,\theta}}{1+h} + 2\frac{\cos\theta}{\sin\theta} - \frac{\Sigma_{,\theta}}{\Sigma}\right) \tag{A.7d}$$
$$g_{\phi\phi,r} = C_{,r} + D_{,r} \tag{A.7e}$$
$$g_{\phi\phi,\theta} = C_{,\theta} + D_{,\theta} \tag{A.7f}$$
$$g_{rr,r} = g_{rr}\left(\frac{\Sigma_{,r}}{\Sigma} + \frac{h_{,r}}{1+h} - \frac{B_{,r}}{B}\right) \tag{A.7g}$$
$$g_{rr,\theta} = g_{rr}\left(\frac{\Sigma_{,\theta}}{\Sigma} + \frac{h_{,\theta}}{1+h} - \frac{B_{,\theta}}{B}\right) \tag{A.7h}$$
$$g_{\theta\theta,r} = \Sigma_{,r} \tag{A.7i}$$
$$g_{\theta\theta,\theta} = \Sigma_{,\theta} \tag{A.7j}$$

$$
\begin{aligned}
g_{tt,rr} =& -h_{,rr}\left(1-\frac{2Mr}{\Sigma}\right)+2Mh_{,r}\frac{\Sigma-r\Sigma_{,r}}{\Sigma^2}-h_{,r}\left(\frac{2Mr}{\Sigma^2}\Sigma_{,r}-\frac{2M}{\Sigma}\right)\\
&-2M\left(1+h\right)\frac{\left(2\Sigma_{,r}+r\Sigma_{,rr}\right)\Sigma-2r\Sigma_{,r}^2}{\Sigma^3}\\
g_{tt,\theta r} =& g_{tt,r\theta}=-h_{,\theta r}\left(1-\frac{2Mr}{\Sigma}\right)+2Mh_{,\theta}\frac{\Sigma-r\Sigma_{,r}}{\Sigma^2}-\frac{2Mr}{\Sigma^2}h_{,r}\Sigma_{,\theta}\\
&-2M\left(1+h\right)\frac{\Sigma\Sigma_{,\theta}-2r\Sigma_{,\theta}\Sigma_{,r}}{\Sigma^3}\\
g_{tt,\theta\theta} =& -h_{,\theta\theta}\left(1-\frac{2Mr}{\Sigma}\right)-4Mrh_{,\theta}\frac{\Sigma_{,\theta}}{\Sigma^2}-2Mr\left(1+h\right)\frac{\Sigma\Sigma_{,\theta\theta}-2\Sigma_{,\theta}^2}{\Sigma^3}\\
g_{t\phi,rr} =& \frac{g_{t\phi,r}^2}{g_{t\phi}}+g_{t\phi}\left[\frac{h_{,rr}\left(1+h\right)-h_{,r}^2}{\left(1+h\right)^2}-\frac{1}{r^2}-\frac{\Sigma_{,rr}\Sigma-\Sigma_{,r}^2}{\Sigma^2}\right]\\
g_{t\phi,\theta r} =& g_{t\phi,r\theta}=\frac{g_{t\phi,\theta}g_{t\phi,r}}{g_{t\phi}}+g_{t\phi}\left[\frac{h_{,\theta r}\left(1+h\right)-h_{,r}h_{,\theta}}{\left(1+h\right)^2}+\frac{\Sigma_{,\theta}\Sigma_{,r}}{\Sigma^2}\right]\\
g_{t\phi,\theta\theta} =& \frac{g_{t\phi,\theta}^2}{g_{t\phi}}+g_{t\phi}\left(\frac{h_{,\theta\theta}\left(1+h\right)-h_{,\theta}^2}{\left(1+h\right)^2}-\frac{2}{\sin^2\theta}-\frac{\Sigma_{,\theta\theta}\Sigma-\Sigma_{,\theta}^2}{\Sigma^2}\right)\\
g_{\phi\phi,rr} =& C_{,rr}+D_{,rr}\\
g_{\phi\phi,\theta r} =& g_{\phi\phi,r\theta}=C_{,\theta r}+D_{,\theta r}\\
g_{\phi\phi,\theta\theta} =& C_{,\theta\theta}+D_{,\theta\theta}\\
g_{rr,rr} =& \frac{g_{rr,r}^2}{g_{rr}}+g_{rr}\left[\frac{\Sigma_{,rr}\Sigma-\Sigma_{,r}^2}{\Sigma^2}+\frac{h_{,rr}\left(1+h\right)-h_{,r}^2}{\left(1+h\right)^2}-\frac{B_{,rr}B-B_{,r}^2}{B^2}\right]\\
g_{rr,\theta r} =& g_{rr,r\theta}=\frac{g_{rr,r}g_{rr,\theta}}{g_{rr}}\\
&+g_{rr}\left[-\frac{\Sigma_{,\theta}\Sigma_{,r}}{\Sigma^2}+\frac{h_{,\theta r}\left(1+h\right)-h_{,r}h_{,\theta}}{\left(1+h\right)^2}-\frac{B_{,\theta r}B-B_{,\theta}B_{,r}}{B^2}\right]\\
g_{rr,\theta\theta} =& \frac{g_{rr,\theta}^2}{g_{rr}}+g_{rr}\left[\frac{\Sigma_{,\theta\theta}\Sigma-\Sigma_{,\theta}^2}{\Sigma^2}+\frac{h_{,\theta\theta}\left(1+h\right)-h_{,\theta}^2}{\left(1+h\right)^2}-\frac{B_{,\theta\theta}B-B_{,\theta}^2}{B^2}\right]\\
g_{\theta\theta,rr} =& \Sigma_{,rr}\\
g_{\theta\theta,\theta r} =& g_{\theta\theta,r\theta}=\Sigma_{,\theta r}=0\\
g_{\theta\theta,\theta\theta} =& \Sigma_{,\theta\theta}
\end{aligned}
$$

Generally in stationary axisymmetric spacetimes expressed in terms of four metric functions g_{tt}, g_{rr}, $g_{\theta\theta}$, $g_{\phi\phi}$ and $g_{t\phi}$ the Chistoffel symbols are expressed as follows.

$$\Gamma^{\theta}{}_{r\theta} = \frac{g_{\theta\theta,r}}{2g_{\theta\theta}} \tag{A.9a}$$
$$\Gamma^{\theta}{}_{tt} = -\frac{g_{tt,\theta}}{2g_{\theta\theta}} \tag{A.9b}$$
$$\Gamma^{\theta}{}_{\phi\phi} = -\frac{g_{\phi\phi,\theta}}{2g_{\theta\theta}} \tag{A.9c}$$
$$\Gamma^{\theta}{}_{\theta\theta} = \frac{g_{\theta\theta,\theta}}{2g_{\theta\theta}} \tag{A.9d}$$
$$\Gamma^{\theta}{}_{rr} = -\frac{g_{rr,\theta}}{2g_{\theta\theta}} \tag{A.9e}$$
$$\Gamma^{\theta}{}_{t\phi} = -\frac{g_{t\phi,\theta}}{2g_{\theta\theta}} \tag{A.9f}$$

$$\Gamma^{r}{}_{rr} = \frac{g_{rr,r}}{2g_{rr}} \tag{A.10a}$$
$$\Gamma^{r}{}_{\theta r} = \frac{g_{rr,\theta}}{2g_{rr}} \tag{A.10b}$$
$$\Gamma^{r}{}_{tt} = -\frac{g_{tt,r}}{2g_{rr}} \tag{A.10c}$$
$$\Gamma^{r}{}_{\theta\theta} = -\frac{g_{\theta\theta,r}}{2g_{rr}} \tag{A.10d}$$
$$\Gamma^{r}{}_{\phi\phi} = -\frac{g_{\phi\phi,r}}{2g_{rr}} \tag{A.10e}$$
$$\Gamma^{r}{}_{t\phi} = -\frac{g_{t\phi,r}}{2g_{rr}} \tag{A.10f}$$

$$\Gamma^{\phi}{}_{rt} = \frac{-g_{tt,r}g_{t\phi} + g_{t\phi,r}g_{tt}}{2\left(g_{tt}g_{\phi\phi} - g_{t\phi}^2\right)} \tag{A.11a}$$
$$\Gamma^{\phi}{}_{\theta t} = \frac{-g_{tt,\theta}g_{t\phi} + g_{t\phi,\theta}g_{tt}}{2\left(g_{tt}g_{\phi\phi} - g_{t\phi}^2\right)} \tag{A.11b}$$
$$\Gamma^{\phi}{}_{r\phi} = \frac{-g_{t\phi,r}g_{t\phi} + g_{\phi\phi,r}g_{tt}}{2\left(g_{tt}g_{\phi\phi} - g_{t\phi}^2\right)} \tag{A.11c}$$
$$\Gamma^{\phi}{}_{\theta\phi} = \frac{-g_{t\phi,\theta}g_{t\phi} + g_{\phi\phi,\theta}g_{tt}}{2\left(g_{tt}g_{\phi\phi} - g_{t\phi}^2\right)} \tag{A.11d}$$

$$\Gamma^{t}{}_{rt} = \frac{g_{tt,r}g_{\phi\phi} - g_{t\phi,r}g_{t\phi}}{2\left(g_{tt}g_{\phi\phi} - g_{t\phi}^2\right)} \tag{A.12a}$$
$$\Gamma^{t}{}_{\theta t} = \frac{g_{tt,\theta}g_{\phi\phi} - g_{t\phi,\theta}g_{t\phi}}{2\left(g_{tt}g_{\phi\phi} - g_{t\phi}^2\right)} \tag{A.12b}$$
$$\Gamma^{t}{}_{r\phi} = \frac{g_{t\phi,r}g_{\phi\phi} - g_{\phi\phi,r}g_{t\phi}}{2\left(g_{tt}g_{\phi\phi} - g_{t\phi}^2\right)} \tag{A.12c}$$
$$\Gamma^{t}{}_{\theta\phi} = \frac{g_{t\phi,\theta}g_{\phi\phi} - g_{\phi\phi,\theta}g_{t\phi}}{2\left(g_{tt}g_{\phi\phi} - g_{t\phi}^2\right)} \tag{A.12d}$$

B. Numerical accuracy

For the integration of geodesic orbits a program has been written using the language C. Two versions were created, both use the 4th order Runge-Kutta algorithm with an adaptive step size. Although we study the reduced system (1.30), we integrate the full geodesic equation

$$\dot{x}^\mu = u^\mu \tag{B.1a}$$

$$\dot{u}^\mu = -\Gamma^\mu{}_{\nu\lambda} u^\nu u^\lambda \tag{B.1b}$$

with the Christoffel symbols and metric and its derivatives in Appendix A.

The step size $\Delta\tau$ is determined by tracking the evolution of $\mathcal{L}$, which is supposed to be an integral of motion, as it is formally equal to the Hamiltonian $\mathcal{H}$. The algorithm tracks the relative error of the Lagrangian

$$\Delta\mathcal{L}_{rel} = \left| \frac{\mathcal{L}(\tau + \Delta\tau) - \mathcal{L}(\tau)}{\mathcal{L}(\tau)} \right| \tag{B.2}$$

and if $\Delta\mathcal{L}_{rel}$ increases above a given maximal value $\Delta\mathcal{L}_{rel}^{max}$, the integration step is halved, if it decreases below a given minimal value $\Delta\mathcal{L}_{rel}^{min}$, the integration step is doubled. This cannot guarantee the accuracy of the overall calculation, which we attempt to monitor by tracking the overall error

$$\Delta\mathcal{L}_{abs} = \left| \frac{\mathcal{L}(\tau) - \mathcal{L}(0)}{\mathcal{L}(0)} \right|. \tag{B.3}$$

The overall time evolution of the errors $\Delta\mathcal{L}_{abs}$ and $\Delta\mathcal{L}_{rel}$ at the N-th point of the surface of section is shown in Fig. B.1. The overall error shows slow numerical drift, which is small compared to the scale of studied phenomena.

The first version is used to study the return mapping of the equatorial plane as described in detail in Chapter 2, the file with the source code is `section.c`. As it integrates the geodesic orbits, it also calculates the rotation angles and the rotation numbers. Using two constants in the beginning of the code, it can be set whether to write points of the Poincaré section and whether to write the rotation angles, which can later be used to calculate the angular dynamical spectra. The center points of the main islands of stability (needed to determine the rotation angles) are determined using an iterative scheme by plotting surfaces of section in small zones around the center up to 9 significant digits. The second version takes no interest in the points where orbits pass through the equatorial plane, it instead evolves the geodesic deviation equation and calculates the FmLCE, the file with the source code is `deviation.c`.

It is also important to note that because of the exponential growth of the deviation vectors their components can reach very large values, which would cause the calculation to lose its accuracy. We make use of the fact that the geodesic deviation equation is linear, so we monitor the deviation vector's length Ξ and renormalize every time it increases above a given boundary. The renormalization procedure consists of simply reducing the vector by a constant factor and calculating the logarithm of the length as a sum of logarithms of the reduction factors and of the current length. This ensures that the calculated values remain as accurate as possible.

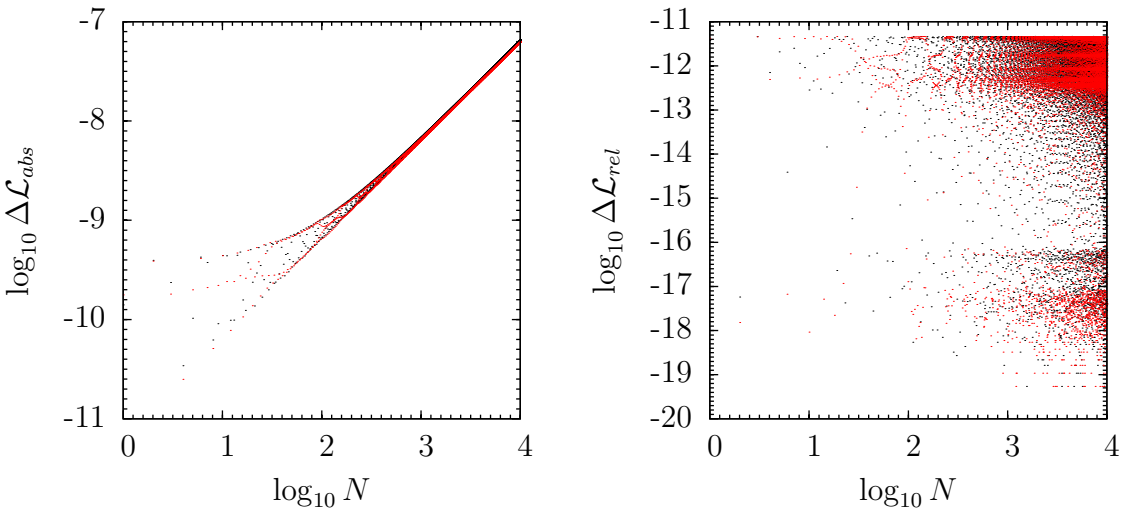

Figure B.1: The error a) $\Delta\mathcal{L}_{abs}$, b) $\Delta\mathcal{L}_{rel}$ evaluated at the N-th point of the surface of section for a regular orbit $r_i = 3.226$ (black) and a chaotic orbit $r_i = 3.2294$ (red), both initial conditions lie on the surface of section for $a = 0.5$, $\epsilon_3 = 0.3$, $E = 0.95$, $L_z = 2.85$.